Missouri University of Science and Technology
Scholars' Mine

Geosciences and Geological and Petroleum Engineering Faculty Research & Creative Works

Geosciences and Geological and Petroleum Engineering

01 Apr 2023

Laboratory Comparative Study of Anionic and Cationic High-Viscosity Friction Reducers in Moderate to Extremely High Total Dissolved Solids Environments

Xiaojing Ge

Abdulmohsin Imqam
Missouri University of Science and Technology, ahikx7@mst.edu

Follow this and additional works at: https://scholarsmine.mst.edu/geosci_geo_peteng_facwork

 Part of the Geological Engineering Commons, and the Petroleum Engineering Commons

Recommended Citation

X. Ge and A. Imqam, "Laboratory Comparative Study of Anionic and Cationic High-Viscosity Friction Reducers in Moderate to Extremely High Total Dissolved Solids Environments," *SPE Journal*, vol. 28, no. 2, pp. 876 - 893, Society of Petroleum Engineers (SPE), Apr 2023.
The definitive version is available at https://doi.org/10.2118/212298-PA

This Article - Journal is brought to you for free and open access by Scholars' Mine. It has been accepted for inclusion in Geosciences and Geological and Petroleum Engineering Faculty Research & Creative Works by an authorized administrator of Scholars' Mine. This work is protected by U. S. Copyright Law. Unauthorized use including reproduction for redistribution requires the permission of the copyright holder. For more information, please contact scholarsmine@mst.edu.

Laboratory Comparative Study of Anionic and Cationic High-Viscosity Friction Reducers in Moderate to Extremely High Total Dissolved Solids Environments

Xiaojing Ge[1] and Abdulmohsin Imqam[1]*

[1]Missouri University of Science and Technology

Summary

High-viscosity friction reducers (HVFRs) have been recently gaining more attention and increasing in use, not only as friction-reducing agents but also as proppant carriers. Reusing produced water has also been driven by both environmental and economic benefits. Currently, most friction reducers on the market are anionic friction reducers, which are fully compatible with most produced water with low to medium level of total dissolved solids (TDS) but show a significant drop at high TDS conditions in terms of their friction reduction performance in most cases. On the contrary, cationic friction reducers are believed to have better TDS tolerance and friction reduction performance under high TDS conditions. However, concerns remain about performance of using anionic and cationic HVFRs with produced water to transport proppant. The ultimate objective of this experimental study is to comparably analyze the proppant transport capabilities of anionic and cationic HVFRs in high TDS and reservoir temperature environments. An anionic HVFR and a cationic HVFR, both at 4 gallons per thousand gallons (GPT), were selected and analyzed. The rheology measurements of these anionic and cationic HVFRs were conducted in deionized (DI) water and high TDS water conditions. Static and dynamic proppant settling tests were conducted at various TDS conditions at reservoir temperature. Wall retardation and particle hindering on the performance of both anionic and cationic HVFRs were also observed and investigated using the particle image velocimetry (PIV) method. The results showed that the anionic HVFR had higher viscosity than the cationic HVFR due to larger molecular weight and had much higher elasticity. Increase in TDS concentration would decrease the viscous and elastic profiles of both anionic and cationic HVFRs. In particular, the elastic profile became negligible for both HVFRs. Besides, the "critical salinity" phenomenon was observed. Above this salinity, the viscosity of HVFRs was no longer affected by increasing TDS level. The "critical salinity" for both of the 4-GPT anionic and cationic HVFRs was in the range of 30 000 to 200 000 mg/L. Moreover, the cationic HVFR had lower "critical salinity" than the anionic HVFR. Finally, the correlation between rheology and proppant transport capabilities of HVFRs is discussed in this paper, and a simplified decision-making process of selecting fracturing fluids is proposed.

Introduction

During the last few years, the industry has been accelerating the adoption of HVFRs to replace traditional fracturing fluids, such as slickwater and guar, in hydraulic fracturing (Hu et al. 2018; Johnson et al. 2018). This is mainly due to several operational and economic advantages of HVFRs, including significantly cutting operational cost with less process and equipment required, exhibiting a higher retained conductivity in the fractured formation, and yielding ideal production improvements in fields (Johnson et al. 2018; Ba Geri et al. 2019). Besides these benefits, the most critical consideration behind using HVFRs in place of traditional fracturing fluids is their proppant-carrying and transporting capability. For traditional slickwater fluid treatment, because the viscosity is too low to suspend the proppant for a sufficient time, the dominant proppant transporting mechanism occurs at a high injection rate. However, even with a significantly high pumping rate, only small and light proppants (40/70 sand, resin-coated sand, and 40/80 lightweight ceramic are the most popular) are pumped with slickwater in the early stages (Palisch et al. 2010). Then, larger and heavier proppants are typically pumped with linear or cross-linked gels, which can better carry and transport this proppant deep into the fractured formation but meanwhile can cause formation damage by the unbroken gel and decrease retained permeability and fracture conductivity (Das and Rahim 2014).

In contrast, the proppant-carrying capability and mechanisms of HVFRs are less understood, let alone quantified (Hu et al. 2018). Moreover, hydraulic fracturing fluids are typically prepared in the field by using fresh water, which can lead to multiple problems in operation, such as the high cost of freshwater acquisition and wastewater disposal, the lack of sufficient freshwater resources near operation sites, etc. These unavoidably bring the industry's attention to the reuse of produced or formation water, which usually has high levels of salinity and hardness. Currently, most high TDS applications are focused on the Marcellus Shale Formation. The Marcellus Shale is a Middle Devonian source rock and retained reservoir which extends across much of the US Appalachian Basin and along five different states including Kentucky, West Virginia, Ohio, Pennsylvania, and New York. It has average reservoir temperature of approximately 140°F (60°C) and bottomhole pressure up to 6,000 psi. The flowback and produced water from this area have a typical high TDS concentration range of 30,000 to 50,000 ppm (Williams et al. 2011; Johnson et al. 2018). To include wider testing of TDS range, two other well-developed formations, Fayetteville Shale and Bakken Formation, are also investigated in this study. Fayetteville Shale is a Mississippian-age, organic-rich shale located in central Arkansas, USA. The play generally comes in at a depth of 4,000–8,000 ft with bottomhole temperature ranging from 120 to 220°F (49–104°C). The concentration of TDS from produced water can be up to 20 000 mg/L (Deville et al. 2011; Kresse et al. 2012; McDonald and Wright 2016). Bakken Formation is a good oil-producing formation in the Williston Basin, which extends across parts of North Dakota, Montana, South Dakota in the

*Corresponding author; email: aimqam@mst.edu

Copyright © 2023 Society of Petroleum Engineers

Original SPE manuscript received for review 10 May 2022. Revised manuscript received for review 2 September 2022. Paper (SPE 212298) peer approved 6 September 2022. Supplementary materials are available in support of this paper and have been published online under Supplementary Data at https://doi.org/10.2118/212298-PA. SPE is not responsible for the content or functionality of supplementary materials supplied by the authors.

Downloaded from http://onepetro.org/SJ/article-pdf/28/02/876/3099587/spe-212298-pa.pdf/1 by Missouri University of Science & Tech user on 09 May 2023

US and Saskatchewan and Manitoba in Canada. The formation water of the Bakken Formation is typically very saline. Based on US Geological Survey produced water database and several other literature sources, the TDS of Bakken Formation ranges from 963 to 343 883 mg/L with average salinity of 285 000 mg/L. The reservoir temperature of Bakken Formation is also high, ranging from 106 to 133°C with average temperature of 123°C (Kurtoglu et al. 2014; Thyne and Brady 2016). Meanwhile, most HVFRs are anionic polyacrylamide (PAM)-based copolymers because of their lower cost and better friction reduction (Ba Geri et al. 2019). However, they are easily affected by fluid salinity and hardness. On the contrary, cationic friction reducers are believed to have better TDS tolerance and performance at high TDS conditions. Moreover, the formation temperature is not always as low as the room temperature (25°C), which may also affect the performance of HVFRs.

The aim of these kinds of fracturing fluid studies is to offer more information for decision-making when selecting fracturing fluids (here, HVFRs) in the field. The general selection process depends on the well location, reservoir formation characteristics, reservoir fluid characteristics, base fluid, and job-design preferences (Loveless et al. 2011). Based on these characteristics, different experimental variables' impacts have been tested and studied. For example, regarding reservoir formation characteristics, studies of fracture wall roughness effects on proppant particle settlings have concluded that settling velocity of proppant is hindered for rough wall configuration (Liu and Sharma 2005; Sahai and Moghanloo 2019; Yamashiro and Tomac 2020). In terms of job-design preferences, proppant property effects on settling velocity have also been experimentally and numerically studied. The proppant property effects include but are not limited to proppant size, proppant shape, proppant density, and proppant concentrations (Zhu et al. 2021). However, most of the research is focused on reservoir formation fluid and base fluid characteristics. The performance of fracturing fluids is directly impacted by viscosity, elasticity, yield stress, rheomalaxis, and the related issue of turbulent drag (Harris et al. 2005). In the presence of salts, the physical and chemical nature of polymer molecules change significantly, which results in rheology properties changing (Nasr-El-Din and Taylor 1996). Shah (1993) studied the rheological characterization of various concentration slurry fluids [i.e., hydrolyzed polyacrylamide (HPAM)] in the range of 2–4 GPT. This study used 20/40 mesh sand with three concentration values varying from 0 to 12 lbm/gal at three temperature conditions (i.e., 80, 100, and 140°F). The collected data showed correlations of apparent viscosity as a function of the fluid concentration, fracture shear rate, temperature, and proppant concentration. Biheri and Imqam (2022) investigated anionic HVFR with guar at various temperatures. The anionic HVFR provides better viscosity and elasticity over the guar at room temperature and temperature up to 50°C. It also showed better sand suspension and transport capacity in both static and dynamic fracture models. Seright et al. (2010) specifically investigated the mechanism behind temperature effect on HPAM polymers. Acrylamide groups within the HPAM polymers would experience hydrolysis to form acrylate groups when temperatures were above 60°C. If the fraction of acrylate groups, which described the degree of HPAM hydrolysis, became too high, HPAM polymers could precipitate, and solution viscosity decreased. However, the performance of test fluids under high TDS formation water was not investigated. Walters et al. (2009) introduced a new clean PAM-based fracturing fluid that is supposed to have high retained conductivity, stable viscosity, low pipe friction, excellent proppant transport, and the capability to be used with produced water. They presented field trials over four wells and found that this fracturing treatment fluid could provide excellent proppant transport with high retained fracture conductivity in tight formations by using formation water. Further research, in regard to TDS effects on polymer, investigates TDS concentrations and different anionic and cationic effects. Shen et al. (2019) comparatively analyzed the common cationic (i.e., Na^+, K^+, Ca^{2+}, and Fe^{3+}) and anionic (SO_4^{2-}) effects on the friction reduction performance of an anionic HVFR and a cationic HVFR. It suggested that cations significantly decreased the friction reduction of the anionic HVFR but had less effects on the cationic HVFR. Besides, K^+ had less impact on friction reduction compared with Na^+. On the contrary, SO_4^{2-} had negligible effects on both anionic and cationic HVFRs in terms of their friction reduction performance. Huh et al. (2009) observed and mentioned the term of "critical salinity." Above this salinity, the viscosity of HPAM would no longer be affected by increasing TDS level, which was because of the limited number of polymer molecules shielded by salt cations. However, neither the mechanism behind these effects nor the effects on proppant transport capability was analyzed. In recent years, the proppant-carrying and transporting mechanisms of HVFRs have also been investigated. Arnipally and Kuru (2018) conducted a comparison study of shear viscosity and elasticity effects on the settling velocity of particles in viscoelastic fluids. At constant shear viscosity conditions, the settling velocity of spherical particles decreased significantly with increasing elasticity. As also occurred under the condition of constant elasticity, the settling velocity of spherical particles decreased significantly when the fluid's shear viscosity was increased. Galindo (2019) conducted a comprehensive study by evaluating the performance of various (approximately 28) commercially available HVFRs, where the test data suggested that the suspension and transport properties of HVFRs were not wholly dependent on fluid viscosity. In contrast, elasticity testing provides the potential to better identify key performance criteria. However, the published research works on cationic friction reducer are still limited (Shen et al. 2019). Moreover, the performance differences of anionic and cationic HVFRs on the proppant transporting under wide range of high TDS conditions and high reservoir temperature were neither qualitatively nor quantitatively investigated.

To address these concerns, the proppant-transporting capability of a PAM-based anionic HVFR was compared with that of a cationic HVFR using both DI water and high TDS formation water from the Fayetteville Shale, Marcellus Shale, and Bakken Formation within 75°C reservoir temperature range. Reservoir temperature of 75°C was selected, which was based on the reservoir temperatures for each formation listed above and the temperature limitation of experimental apparatus, and to mimic the closest reservoir condition. Much denser 30/60 intermediate ceramic proppant was selected to make distinction between sand proppant used in traditional fracturing fluid treatments and also to avoid proppant shape effects on settling velocity. Wall retardation effect and particle-hindered effect on the performance of both anionic and cationic HVFRs were also investigated using the PIV method.

Experimental Materials and Description

Experimental Materials. ***Preparing HVFR Fracturing Fluids.*** An anionic PAM (FLOJET DRP 2340X) and a cationic PAM (FLOJET DRP 419X), provided by SNF Holding Company, were selected to prepare HVFRs. Both HVFRs were in the form of dry powder and needed to be hydrated prior to testing. Concentration of 4 GPT (around 0.127% by weight for dry HVFRs) was chosen, which was the common HVFR concentration used in the fields (Ba Geri et al. 2019). DI water was used to prepare the polymer solutions. American Chemical Society grade salts ($CaCl_2{\cdot}2H_2O$, $MgCl_2{\cdot}6H_2O$, $MgSO_4$, KCl, NaCl, and $SrCl_2$) were used to prepare the synthetic high TDS formation fluids for Fayetteville Shale, Marcellus Shale, and Bakken Formation with typical TDS of 10 000 mg/L (Kresse et al. 2012), 30 000 mg/L (Johnson et al. 2018), and 200 000 mg/L (Kakadjian et al. 2015), respectively. To minimize different cationic and anionic effects on HVFRs but meanwhile mimic closest formation water conditions, salts (which existed in all three formation waters) were selected and prepared. Other uncommon and low concentration salt components for each formation were just ignored. Therefore, all three synthetic formation fluids had exactly the same components but at different concentrations. The composition of each formation water is shown in **Table 1**.

Downloaded from http://onepetro.org/SJ/article-pdf/28/02/876/3099587/spe-212298-pa.pdf/1 by Missouri University of Science & Tech user on 09 May 2023

Components	Concentration (ppm)		
	Fayetteville Shale Formation Water	Marcellus Shale Formation Water	Bakken Formation Water
Sodium	1,400	9,620	76,600
Potassium	300	440	500
Calcium	950	2,650	13,500
Magnesium	1,800	100	1,100
Strontium	400	400	700
Chloride	3,000	16,780	107,000
Sulfate	2,150	10	600
TDS	10,000	30,000	200,000

Table 1—Composition of salt contents in synthetic Fayetteville Shale formation water, Marcellus Shale formation water, and Bakken formation water.

HVFR solutions were mixed for 2 hours with a rotational speed of 600 rev/min to have a good vortex with no air bubbles. To recreate the same test conditions for all prepared fluids, all rheology measurements were conducted directly after mixing to avoid any viscosity changes due to polymer hydrolysis (Nasr-El-Din and Taylor 1996). The average pH of anionic and cationic HVFR fluids was 7.5 and 4.6, respectively. The average density of testing fluids was 1.2 g/cm^3. All tests were repeated three times, and the two closest values were averaged and reported.

Proppant. The 30/60 (250–600 μm) intermediate ceramic proppant with specific gravity (SG) = 3.27 was used to conduct both static and dynamic settling experiments. One of the reasons for choosing this proppant was to better control experimental variables. According to Zhu et al. (2021), the settling velocity of proppant was strongly affected by its shape (i.e., sphere, cylinder, and cube), diameter, density, and particle Reynolds number. Compared with traditional silica sand, ceramic proppant was more uniform in size and shape (Liang et al. 2016). Another important reason is to make distinction between proppant used in traditional fracturing fluid treatments like slickwater fracturing. In the early stages of slickwater treatment, only small and light proppants (40/70 sand, resin-coated sand, and 40/80 lightweight ceramic are the most popular) are pumped with fracturing fluids (Palisch et al. 2010).

Rheometer. A high-accuracy advanced rheometer (Anton Paar, MCR 302) with a parallel-plate system was run for both anionic and cationic HVFR fracturing fluid rheology. The rheometer had a minimum torque rotation of 1 nNm, and a normal force ranges from 0.005 to 50 N. A parallel-plate measuring system (PP50, using a 0.30-mm gap) was used to measure the viscosity shear profile, normal forces, and dynamic oscillatory shear measurements at laboratory temperature and high-temperature conditions. The rheometer had a temperature control system, which enabled temperature-dependent measurements up to 200°C. A cover was used to prevent evaporation for testing samples at elevated temperature conditions over long periods (e.g., 50 and 75°C).

Rheological Characterization of HVFRs. ***Flow Curve Measurement.*** The viscosities and apparent normal stress differences (N1−N2) of fracturing fluids were measured in a shear rate sweep using 25-mm parallel-plate geometry at a 30-μm gap. The shear rate varied from 0 to 1000 s^{-1}. Isothermal single shear rate tests were run at a constant shear rate of 84.5 s^{-1} for 100 minutes at three temperature settings of 25, 50, and 75°C to investigate thermal stability of fluid samples.

Oscillatory Shear Profile Measurement. The dynamic oscillatory shear measurements were conducted to measure the elasticity profiles, including the storage modulus G', loss modulus G'', and relaxation time. Before implementing the oscillatory shear tests, amplitude sweep tests were carried out to determine the limit of the linear viscoelastic (LVE) region for each test sample. Then, strain value of 1% (0.01), which was within the limit of the LVE region for all test samples, was selected for further oscillatory shear tests. The oscillatory test was implemented over a range of angular frequencies from 0.01 to 100 rad/s and temperature setting of 25°C.

Proppant Settling Velocity Experiment Setup and Measurement. ***Proppant Static Settling Velocity Measurement and PIV Analysis.*** Fig. S-1a in the Supplementary Material shows the setup for the unconfined settling velocity measurement. The experiment was performed in a 100-mL transparent glass cylinder tube with a diameter much larger than the proppant diameter to ensure that the proppant settling velocity was not influenced by the wall of the glass container. The ratio of the proppant diameter to the glass diameter was approximately 1:50 to 1:120, which was acceptable to avoid any effect of the glass wall.

Fig. S-1b shows the confined rectangular model with the length of 60 cm and the fracture width of 3.5 mm. Rubbers placed between the parallel glasses were used to represent the fracture width. The ratio of the proppant diameter to the fracture width was approximately 1:6 to 1:14. Two parallel visible glasses with smooth wall roughness allowed a high-resolution camera to capture the proppant settling process.

The 30/60 intermediate ceramic proppant with SG = 3.27 was used to measure the proppant terminal settling velocity. For static single proppant settling, unconfined and confined containers were filled with the test fluids (around 160 mL for both containers), and a proppant sample was immersed in the fluid and allowed to settle. The settling length of investigation was 22.5 and 52 cm for the unconfined apparatus and confined apparatus, respectively. For static multiproppant settling, approximately 160 mL of testing fluids were mixed with 1 ppg concentration of proppant in a beaker first, and then were slowly poured into the unconfined model. The settling length of investigation was 17 cm to avoid proppant sedimentation part at the bottom of the tube. A meter stick was placed alongside the cell, and the settling process was captured using a high-resolution video camera. The recorded video was then used to track the position of the particle and measure the terminal settling velocity. The software application Tracker 2.0 was used to obtain accurate measurements of the single proppant settling velocities. OpenPIV was used to measure multiparticle settlings. OpenPIV software uses the PIV method to obtain the particle displacement data from digital images. Images between small time intervals can be extracted as frames from the video recorded with a high-speed camera. The digital image was first divided into a number of meshes (interrogation regions) based on image sizes. Then, the OpenPIV software found the same or similar mesh within the next digital image. Finally, particle displacements and velocities were obtained by comparing particles' positions between two subsequent frames. The rheological properties of the fluid were measured as illustrated in the previous section, and the density of the fluid was measured using an accurate weighing balance. The effect of temperature

Downloaded from http://onepetro.org/SJ/article-pdf/28/02/876/3099587/spe-212298-pa.pdf/1 by Missouri University of Science & Tech user on 09 May 2023

on the settling velocity was also investigated using a laboratory water bath. At least three measurements were made for each reported settling velocity under different temperatures and TDS conditions.

Dynamic Proppant Transport Analysis. Fig. S-1c in the Supplemental Material shows the dynamic transport fracture model that was built to simulate proppant slurry transport in hydraulic fracturing treatments. A laboratory fracture model of 2×2 ft was constructed with visible glasses with smooth wall roughness as a slot model with a gap of 0.25 in. Four injection points representing four perforations of 0.25-in. diameter were made perpendicular to the fracture slot. Each injection point was connected to a pressure indicator. Only one of the four perforations (at the bottom of the model) was used to conduct the proppant transport. A drum blanket heater controlled the fracture fluids' temperature at 75°C. A flow-rate meter was joined to a high-temperature centrifugal sump pump, and a valve was placed between the pump and the flowmeter to obtain the desired flow rate as the proppant was added and temperature increased.

The 4-GPT anionic and cationic HVFRs were prepared using a mechanical blender in both DI and high TDS conditions. Each test required 5 gal of fracture fluids, which made the volume of dynamic fracture model to the drum volume of fluid around 1:12. All prepared fracturing fluids were left for 1 day to ensure there were no air bubbles in the fluids before using. To mimic an HVFR stimulation treatment in a reservoir, the fracturing fluid was first heated to the desired temperature of 75°C and injected into the fracture slot as shown in Fig. S-1c. After the fluid level inside the dynamic model became stable, the video camera began filming with a speed of 30 frames per second. The fracture slot apparatus was illuminated with an LED vapor tight fixture (4,000 lumens, 2×2 ft) to add extra light during recording. Then, 5 lb of 30/60 ceramic proppant, which was 1 ppg concentration in the slurry, were injected into the dynamic fracture model. The pumping of the slurry continued for half an hour to allow adequate time to evaluate the capability of the HVFRs to transport the proppant. All the experiments were conducted using a constant pumping rate of 2 gal/min. During the pumping process, the slurry was stirred continuously to prevent sedimentation of proppant on the bottom of the drum and recycled into the drum once it flowed out of the dynamic fracture model.

Experimental Scope

The general experimental scopes of this research study are shown on **Fig. 1**. The rheology properties and proppant transport capabilities of both anionic and cationic HVFRs were comparatively studied under various TDS concentrations and high reservoir temperature. The correlation between rheology data and proppant settling experiments specifically are discussed.

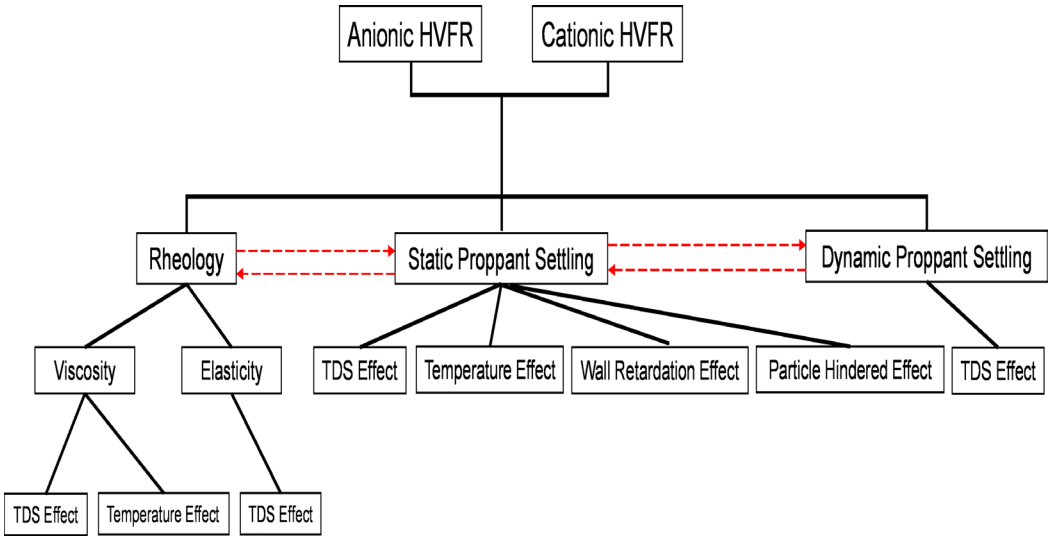

Fig. 1—Experimental scope of this research study.

Results and Discussion

Viscosity Measurement Tests. ***Effect of TDS.*** Typically, the produced water is classified into five types based on the concentration of the TDS. Fresh water usually has a TDS concentration of less than 1000 mg/L. Slightly saline water has a TDS concentration ranging from 1000 to 3000 mg/L. Moderately saline water has a TDS concentration ranging from 3000 to 10 000 mg/L. Saline water has a TDS concentration ranging from 10 000 to 35 000 mg/L. For TDS concentrations above 35 000 mg/L, the fluid is classified as seawater (Downey and Armstrong 1977). The waters produced by the Fayetteville Shale, Marcellus Shale, and Bakken Formation typically have TDS concentrations of approximately 10 000, 30 000, and 200 000 mg/L, respectively, which are moderate to high. Currently, most HVFRs used in fields are anionic, so they are usually affected by the TDS in the water source. The negative charges from the carboxyl groups of the HVFR will be shielded by cations in the formation water and inhibit the repulsive interaction between the negative charges. In this experiment, an anionic friction reducer and a cationic friction reducer were comparatively investigated.

Steady shear viscosity measurements were made for all the fluid mixtures using an advanced rheometer. **Fig. 2** shows the viscosity (μ) as a function of the shear rate ($\dot{\gamma}$) for 4-GPT HVFRs in DI water and high TDS formation water at 25°C (i.e., room temperature). All the tests were run from 0.1 to 1000 s^{-1} and also from 1000 to 0.1 s^{-1} to determine if there were any fluid structural changes during the shear viscosity tests (solid fill markers for viscosity from 0.1 to 1000 s^{-1} and no fill markers for viscosity from 1000 to 0.1 s^{-1}). Shear rates usually vary from 10 to 100 s^{-1} in the near-wellbore region and fractures (Haghshenas and Nasr-El-Din 2014). Within the experimentally accessible window (i.e., 10–100 s^{-1}), HVFRs exhibited shear-thinning behavior in DI water condition and the viscosity profiles of the shear rate from low to high and also from high to low aligned well, which means there were no fluid structural changes for either the anionic or cationic HVFR during shearing. Also, the anionic HVFR had viscosity almost twice as high as its cationic counterpart.

Downloaded from http://onepetro.org/SJ/article-pdf/28/02/876/3099587/spe-212298-pa.pdf/1 by Missouri University of Science & Tech user on 09 May 2023

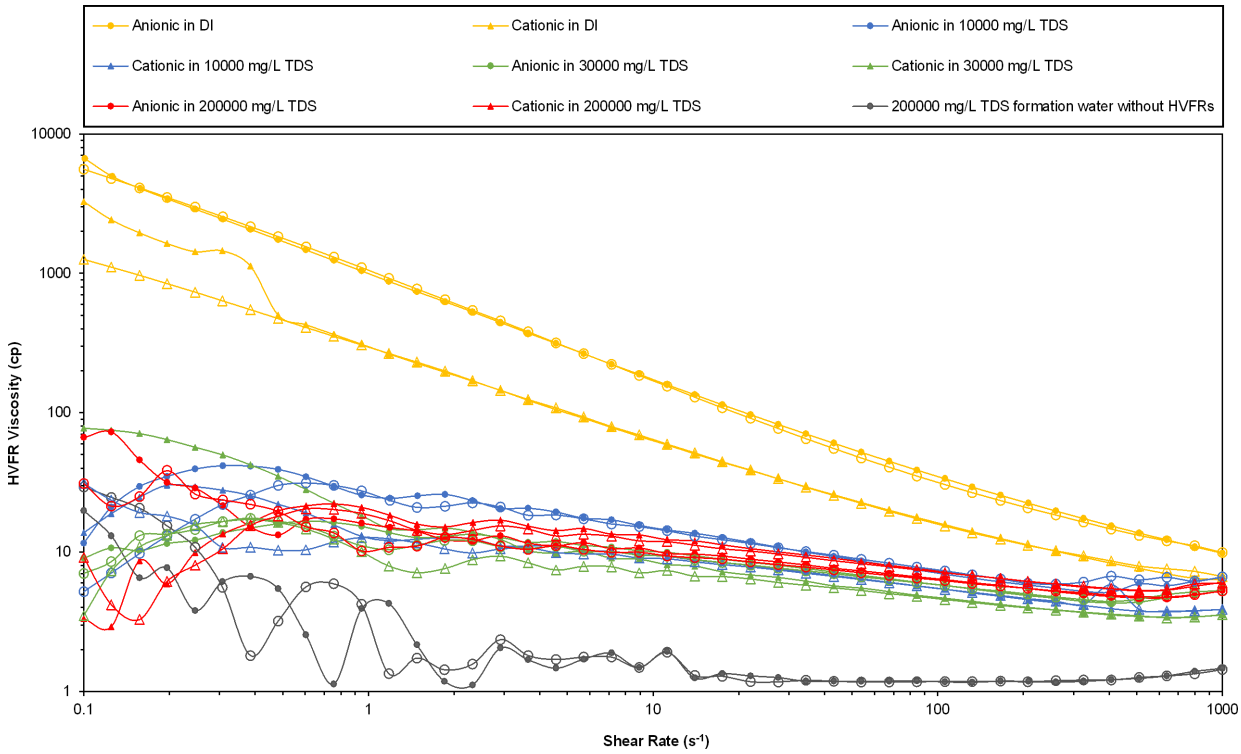

Fig. 2—Viscosity of the 4-GPT anionic and cationic HVFRs in DI water and 10 000-, 30 000-, and 200 000-mg/L TDS formation waters at 25°C.

At high TDS formation water conditions, the viscosities of the fluids decreased significantly and were very close to each other. To identify the differences more clearly, the viscosity profiles of both HVFRs with high TDS formation water within accessible shear rate window were plotted on **Fig. 3**, using 200 000-mg/L TDS formation water without HVFR as a benchmark. The viscosity of pure TDS formation water was approximately 1 cp along the whole shear rate range. HVFRs played an important role in adding viscosity to fluids, even at extremely high TDS conditions. At 10 000-mg/L formation water condition, high TDS significantly decreased the viscosity of both anionic and cationic HVFRs by a factor of 4 and 3, respectively. At 30 000-mg/L formation water condition, viscosity decreased by a factor of 6 for the anionic HVFR and a factor of 4 for the cationic HVFR. In other words, high TDS (up to 30 000 mg/L here) had a more pronounced effect on the viscosity of the anionic HVFR than the cationic HVFR, even though the anionic one still had higher average values. However, when the TDS increased up to 200 000 mg/L, the viscosity of both fluids increased to only slightly less than the viscosity of the anionic HVFR in 10 000- mg/L TDS formation water. Moreover, the cationic HVFR had higher viscosity than the anionic one. This phenomenon was mainly due to the critical salinity.

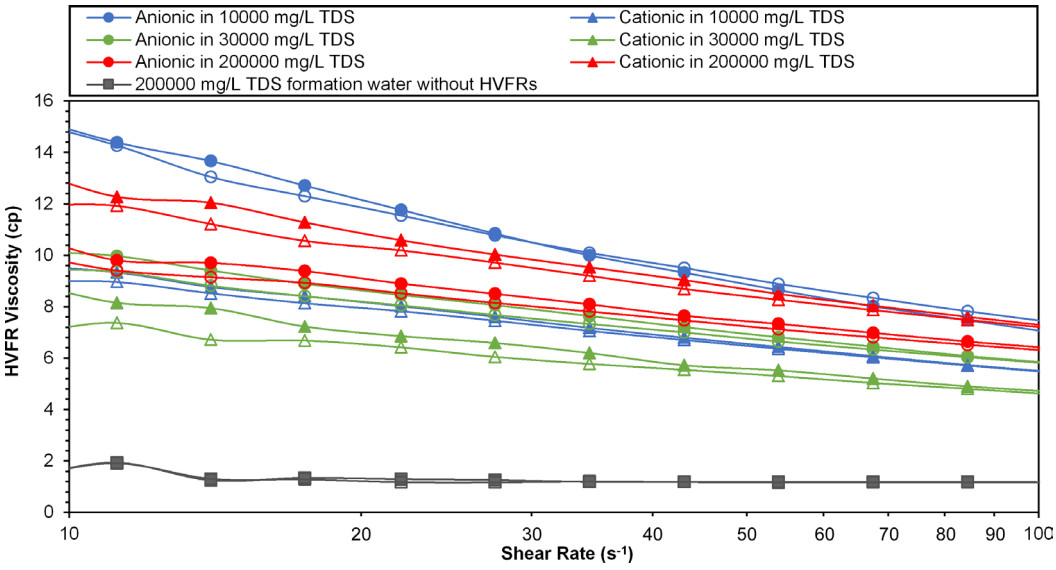

Fig. 3—Viscosities of the 4-GPT anionic and cationic HVFRs in 10 000-, 30 000-, and 200 000-mg/L TDS formation water and pure 200 000-mg/L TDS formation water without HVFRs at 25°C within experimental accessible window.

Downloaded from http://onepetro.org/SJ/article-pdf/28/02/876/3099587/spe-212298-pa.pdf/1 by Missouri University of Science & Tech user on 09 May 2023

Fig. S-2a in the Supplementary Material shows a typical structure of HPAM, consisting of monomers of anionic carboxylic groups. With DI water, the anionic HPAM backbone was fully stretched because of the negative charges of the acrylic acid moieties repelling each other. The repulsion resulted in the stretching of the polymer chain and a high viscosity yield. However, when salts are present, the anionic carboxylic groups would react with monovalent and multivalent cations such as Na^+ and Ca^{2+}. Fig S-2b shows three main interactions between cations (i.e., Ca^{2+} here) and carboxylic groups, including intrachain, interchain, and large aggregate. These reactions decreased the repulsions between the anionic carboxylic groups and made polymer molecules not fully stretched. Besides, they might also lead to the precipitation from the solution. All these reduced the viscosity of the anionic HVFR (Ward and Martin 1981). Similarly for the cationic HVFR, anions like Cl^- and SO_4^{2-} decreased the repulsive forces within the polymer, which reduced its viscosity (Giraldo et al. 2016). With increasing TDS level (i.e., from 10 000 to 30 000 mg/L), cations occupied more of the anionic groups on polymer backbones for the anionic HVFR (or anions occupied more of the cationic groups on polymer backbones for the cationic HVFR), inducing lower viscosity levels. At critical salinity (somewhere between 30 000 and 200 000 mg/L), the charged groups of HVFRs were fully shielded and the net charge equaled to zero. Further TDS increases resulted in repulsions and re-expanding the polymeric chains in solution, which increased viscosity of HVFRs. Besides, salts themselves also had generally positive effects on the viscosity of water, even though these effects were small (Applebey 1910). Moreover, the cationic HVFR might have lower critical salinity than the anionic HVFR. This explained why the cationic HVFR had higher viscosity than the anionic HVFR in 200 000-mg/L TDS formation water. However, whether cations had more effects on the anionic HVFR, or anions had more effects on the cationic HVFR needs to be further investigated. Overall, the viscosity of the test fluids with high TDS decreased only slightly with increasing shear rates, enabling them to be more confidently interpreted as "close-Newtonian."

Power-Law Model. The power-law model ($\mu = K\,\dot{\gamma}^{n-1}$) is fitted to the data in the range of the shear rates from 10 to 100 s^{-1}, where μ is the apparent viscosity (mPa·s); K is the power-law constant (mPa·s^n); $\dot{\gamma}$ is the shear rate (s^{-1}); and n is the power-law index (dimensionless). The viscosity and shear rate relationship for all prepared test fluids followed the power-law model. The power-law parameters are given in **Table 2**. For both the anionic and cationic HVFRs in high TDS formation water, the deviations of n values from unity were much smaller compared with the HVFRs in DI water conditions, which indicate the more "Newtonian-like" behavior of fluids.

Concentration (GPT)	K (mPa·s^n)	n	R^2
Anionic at DI water	848.75	0.302	0.9992
Cationic at DI water	241.93	0.409	0.9992
Anionic at 10 000-mg/L TDS	32.252	0.671	0.9987
Cationic at 10 000- mg/L TDS	16.433	0.764	0.9973
Anionic at 30 000- mg/L TDS	17.547	0.763	0.9974
Cationic at 30 000- mg/L TDS	15.389	0.742	0.9954
Anionic at 200 000- mg/L TDS	16.722	0.793	0.9925
Cationic at 200 000- mg/L TDS	22.713	0.754	0.9974

Table 2—Power-law parameters of the 4-GPT anionic and cationic HVFRs at 25°C.

Effect of Temperature. To investigate the stability of the anionic and cationic HVFRs at 25, 50, and 75°C in DI water and high TDS formation water, isothermal single shear rate tests were run at a shear rate of 84.5 s^{-1}. **Fig. 4** indicates the change in viscosity over time at each test temperature. At ambient temperature, all test fluids showed constant viscosity over time. At 50°C, the viscosity slightly decreased over time for both anionic and cationic HVFRs at DI water condition. With high TDS formation water, viscosity decreased more sharply, and this effect became even more significant for the anionic HVFR. As shown in **Fig. 4b**, the anionic HVFR had higher viscosity than the cationic HVFR in both 30 000- and 200 000- mg/L TDS levels at the beginning of tests. However, over time, the viscosity of the anionic HVFR became lower than the viscosity of the cationic one. At 75°C, the viscosity decreased significantly over time for both DI water and high TDS formation water conditions. Similar to the results of 50°C, this effect became even more significant for the anionic HVFR. As shown in **Fig. 4c**, the anionic HVFR had higher viscosity than the cationic HVFR in both 10 000- and 30 000- mg/L TDS levels at the beginning of tests. With time increasing, the viscosity of the anionic HVFR became lower than the viscosity of the cationic one. At 200 000-mg/L TDS formation water condition, the viscosity profiles of both HVFRs became unusually high and fluctuating, which might be due to the solution evaporation and precipitation of salt solids at high temperature. To prevent this, a magnetic sample cover should be used in future tests when measuring samples containing solvents. In general, high TDS concentration increased the temperature effect on the thermal stability of HVFRs, and this effect was more significant for the anionic HVFR.

Elasticity Measurement Tests. Elasticity measurements were conducted for both anionic and cationic HVFRs at a variety of TDS conditions. In this section, normal stress and oscillatory shear test results are presented.

Effect of TDS. *Normal Stress Tests.* Normal stress is a very sensitive and accurate tool for material elasticity measurements and can generate useful information about the internal structure to the material's flow behavior. Apparent normal stress (N_1) is the cause of the extra drag on the proppant when settling (Padhy et al. 2013). **Fig. 5** displays the apparent normal stress profiles from 500 to 1000 s^{-1} for HVFRs in DI water and high TDS formation water at 25°C (i.e., room temperature), using 200 000-mg/L TDS formation water without HVFRs as a benchmark. All test fluids showed relatively small and negative values for a shear rate below 600 s^{-1} because those test fluids, especially lower-viscosity fluids, do not generate appreciable axial force until the shear rate grows high enough. For shear rates above 600 s^{-1}, the anionic HVFR in DI water generated significant normal stress (positive value) upon shearing. In addition, the normal stress for the anionic HVFR increased due to shearing. This also suggests that no breakage or degradation of the polymer chains occurred as a result of the high shear rates. The anionic HVFR in 10 000- mg/L TDS formation water also generated positive normal stress when shear rate was around 1000 s^{-1} but lower than the normal stress of the anionic HVFR in DI water. When TDS concentration was equal to or above 30 000 mg/L, the normal stress of the anionic HVFR was negative along the whole shear rate ranges. The cationic HVFR only

Downloaded from http://onepetro.org/SJ/article-pdf/28/02/876/3099587/spe-212298-pa.pdf/1 by Missouri University of Science & Tech user on 09 May 2023

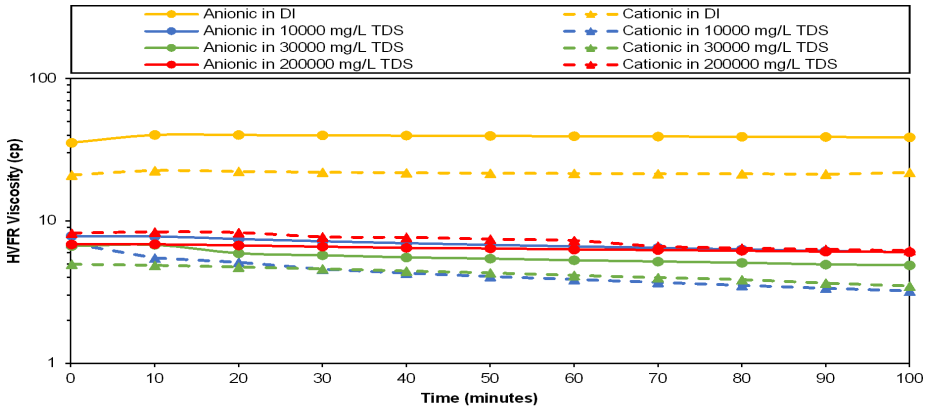

(a) Viscosity measurements 25°C

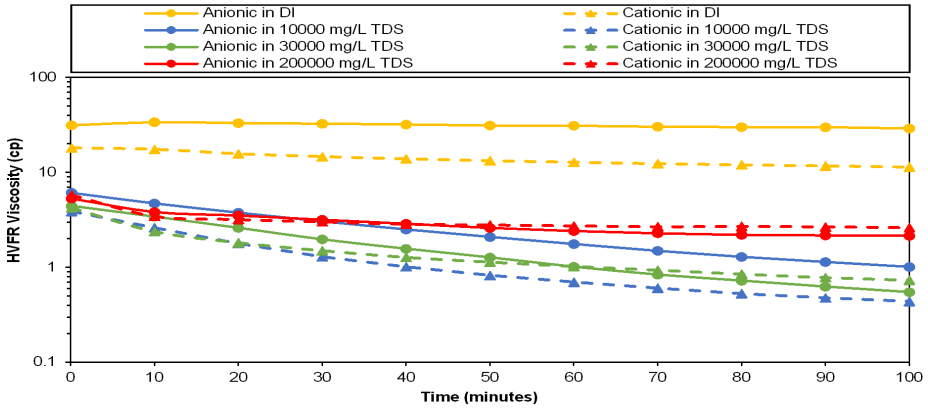

(b) Viscosity measurements 50°C

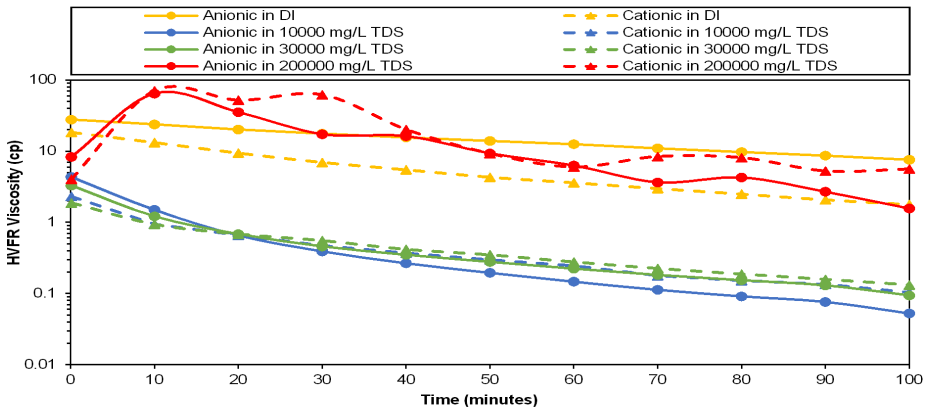

(c) Viscosity measurements 75°C

Fig. 4—Isothermal single shear rate test of the 4-GPT anionic and cationic HVFRs at 84.5 s^{-1} in DI water and high TDS formation water at (a) 25, (b) 50, and (c) 75°C.

generated negative values of normal stress in both DI water and high TDS formation water conditions and even as low as the normal stress of pure 200 000-mg/L TDS formation water, which was known as nonviscoelastic fluid. This results from sampling inertia causing the fluid sample to move away from the axis of rotation, demonstrating the negligible elastic properties of both anionic and cationic HVFRs under high TDS formation water conditions.

Oscillatory Shear Tests. The elasticity of fluids is also quantified by dynamic oscillatory shear measurements, which are made over a range of frequencies from 0.01 to 100 rad/s. **Fig. 6** shows the elastic modulus, G', and the viscous modulus, G'', as functions of the angular frequency, ω, for both the anionic and cationic HVFRs in DI water and high TDS formation water at 25°C ambient temperature. For both HVFRs in DI water, the G'' values were higher than the G' values at the beginning of the experiments. This is because the HVFRs are more viscous fluids than they are elastic. When $G''(\omega)$ and $G'(\omega)$ are equal, the crossover points for each concentration are marked in **Fig. 6**, and the ω values are presented in **Table 3**. Then, the relaxation time, T, can be calculated by inverting ω, which is also shown in **Table 3**. The relaxation time is a measure of the elasticity of a fluid. A fluid with zero relaxation time is referred to as an inelastic fluid, and the elasticity of the fluid is greater if it has a longer relaxation time. The anionic HVFR showed a nearly four times higher relaxation time than the cationic HVFR in DI water under ambient temperature condition. At high TDS formation water conditions, high TDS

Downloaded from http://onepetro.org/SJ/article-pdf/28/02/876/3099587/spe-212298-pa.pdf/1 by Missouri University of Science & Tech user on 09 May 2023

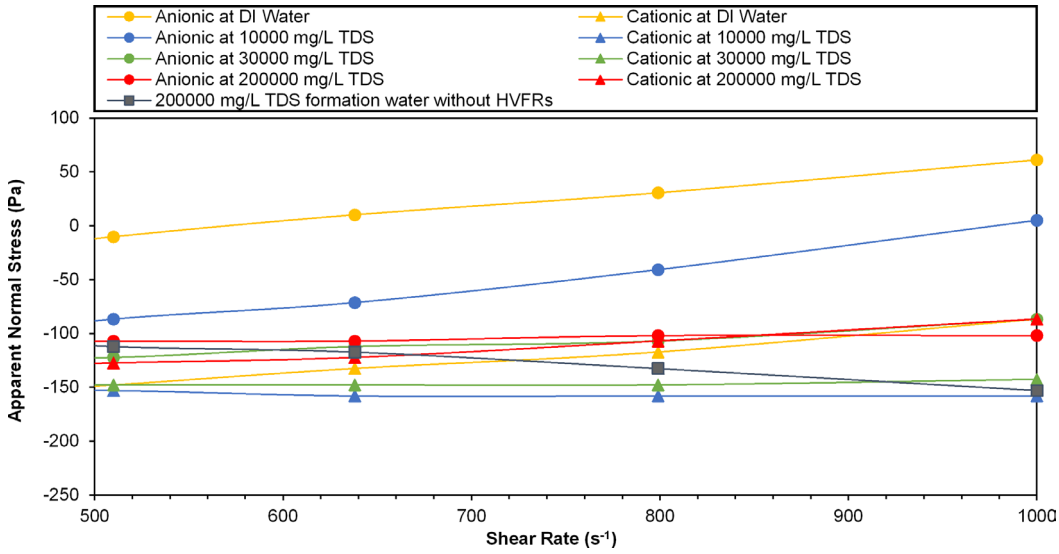

Fig. 5—Apparent normal stress of the 4-GPT anionic and cationic HVFRs in DI water and high TDS formation water as well as the normal stress of pure 200 000-mg/L TDS formation water without HVFRs at 25°C.

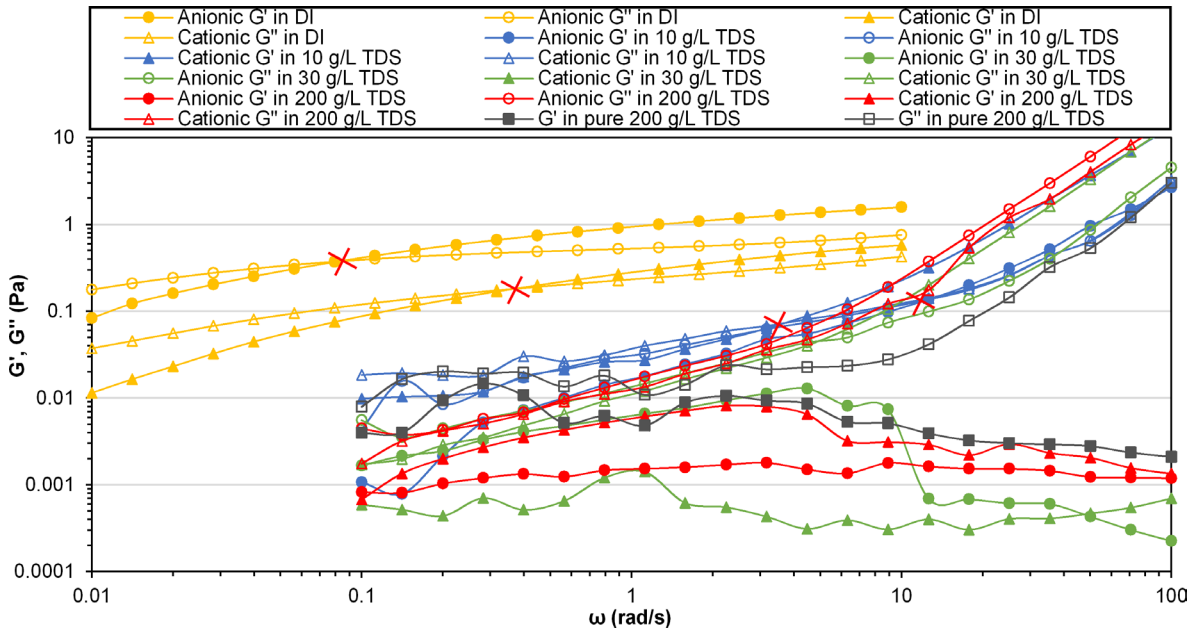

Fig. 6—Oscillatory shear measurement of the 4-GPT anionic and cationic HVFRs in DI water and high TDS formation water as well as the pure 200 000-mg/L TDS formation water without HVFRs at 25°C.

significantly decreased both G' and G'' for HVFRs at an angular frequency from 0.1 to 10 rad/s. G' and G'' of all test fluids were within 0.0001–0.1 region and fairly small. At 10 000-mg/L TDS level, both the anionic and cationic HVFRs showed much smaller relaxation time compared with the DI water condition. When the TDS level reached to 30 000 mg/L, G'' became dominant, and there were huge differences between G' and G'' for both HVFRs, which means the elasticity of fluids was negligible. Besides, there was no crossover for both anionic and cationic HVFRs within the 0.1–100 rad/s angular frequency region. To sum up, the anionic HVFR was much more elastic than the cationic HVFR in DI water conditions and high TDS significantly decreased the elasticity of HVFRs, which indicated consistent results as apparent normal stress. According to Panyukov (2020), the elastic properties of polymer highly depend on the molecular structures of the polymer network (or entanglements) and the polydispersity of its strands. High TDS tended to change entanglements of HVFRs, which resulted in decreasing of elasticity. Several previous studies suggested to hydrophobically modify traditional HPAM by adding hydrophobic monomers to the polymer backbone to improve its viscoelastic performance (Løbø Viken et al. 2016). However, the mechanism of controlling elasticity of HVFRs needs further investigation. In addition, G' and G'' of pure 200 000-mg/L TDS formation water without HVFRs were tested as benchmarks, which showed similar results as HVFRs in high TDS formation water and demonstrated that the elasticity of both the anionic and cationic HVFRs was negligible again. Moreover, it was challenging to measure G' and G'' for low-viscosity fluids (i.e., HVFRs in high TDS formation water). The rheometer used in this experimental study was combined motor transducer. However, it was much better to use separate motor transducer rheometers to perform oscillatory measurements on low-viscosity fluids due to lower system inertia contribution according to Franck (2003).

Downloaded from http://onepetro.org/SJ/article-pdf/28/02/876/3099587/spe-212298-pa.pdf/1 by Missouri University of Science & Tech user on 09 May 2023

Fluids	Crossover, ω (rad/s)	Relaxation time, T (seconds)
Anionic at DI	0.0828	12.077
Cationic at DI	0.371	2.695
Anionic at 10 ooo-mg/L TDS	12.5	0.080
Cationic at 10 000-m g/L TDS	3.67	0.272
Anionic at 30 000-m g/L TDS	N/A	N/A
Cationic at 30 000-mg/L TDS	N/A	N/A
Anionic at 200 000-mg/L TDS	N/A	N/A
Cationic at 200 000-mg/L TDS	N/A	N/A
200 000-mg/L TDS without HVFRs	N/A	N/A

Table 3—Loss modulus and storage modulus crossover points and relaxation times of the 4-GPT anionic and cationic HVFRs in DI and high TDS formation water as well as the pure 200 000-mg/L TDS formation water without HVFRs at 25°C.

Effect of Hydration Time. Hydration time might also affect the rheology performance of both the anionic and cationic HVFRs, especially in the absence of continuous shear rate and presence of high TDS. According to SNF Holding Company, the general stability time of anionic and cationic HVFRs prepared in DI water was around 1 week and 1 day, respectively. **Fig. 7** shows the viscosity and elasticity profiles of the cationic HVFR in DI water with hydration times of 2 hours and 1 week. The crossover points for G' and G'' are marked in **Fig. 7b**. The cationic HVFR in DI water with 1 week of hydration time had slightly higher viscosity and elasticity profiles than the one with only 2 hours of hydration time. However, based on the research presented in Abdullah et al. (2008), increasing hydration time would decrease viscosity of the polymer and further reduce its drag reduction. Therefore, more hydration time tests on HVFRs with both DI water and high TDS formation water were needed.

As per our research, because all rheology tests were conducted after 2-hour mixing, hydration time effect was negligible.

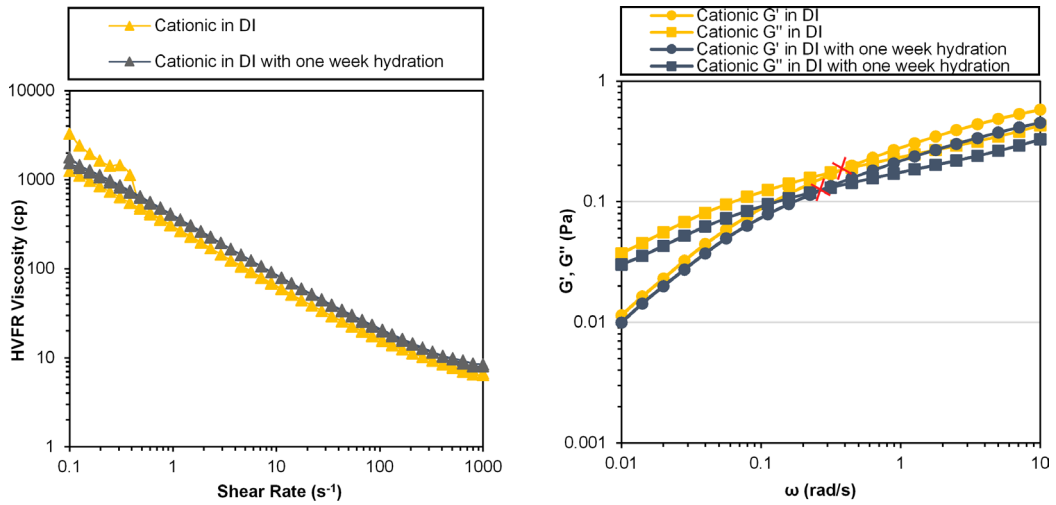

(a) Viscosity tests (b) Oscillatory shear tests

Fig. 7—(a) Viscosity and (b) elasticity of the 4-GPT cationic HVFR in DI water at 25°C for hydration times of 2 hours and 1 week.

Static Settling Velocity Measurement. ***Effect of TDS.*** **Fig. 8** compares the unconfined settling velocities of HVFRs to understand the impact of the TDS. With DI water, anionic and cationic HVFRs can fully suspend the proppant with 0- and 0.07- cm/s settling velocity, respectively; with 10 000- mg/L TDS formation water, the average settling velocity jumped from 0 to 1.2 cm/s for the anionic HVFR and from 0.07 to 2.1 cm/s for the cationic HVFR; with 30 000- mg/L TDS formation water, the average settling velocity jumped from 1.2 to 1.9 cm/s for the anionic HVFR and from 2.1 to 2.9 cm/s for the cationic HVFR; with 200 000-mg/L TDS formation water, the average settling velocity slightly increased from 1.9 to 2.4 cm/s for the anionic HVFR but dropped from 2.9 to 1.9 cm/s for the cationic HVFR. The results matched previous rheology tests very well. At DI water condition, both the anionic and cationic HVFRs showed good proppant suspension capability due to high-viscosity and elasticity profiles. As high TDS presented, viscosity of both HVFRs sharply reduced and elasticity became negligible, which resulted in significant increasing of proppant terminal settling velocity. Besides, due to relatively higher viscosity, the anionic HVFR had lower settling velocity than the cationic HVFR. With TDS level increasing, the terminal settling velocity also increased. Once the TDS level was above "critical salinity" and reached 200 000 mg/L, settling velocity only increased slightly for the anionic HVFR but decreased for the cationic one. Moreover, settling velocity of the cationic HVFR with 200 000- mg/L TDS formation water was even lower than the anionic one as a result of relatively low critical salinity.

Downloaded from http://onepetro.org/SJ/article-pdf/28/02/876/3099587/spe-212298-pa.pdf/1 by Missouri University of Science & Tech user on 09 May 2023

Effect of Temperature. **Fig. 9** presents the temperature effects on the settling velocity of HVFRs in DI water and high TDS formation water. In **Fig. 9a**, curves were fluctuating due to relatively small settling velocity values. With DI water, settling velocities of HVFRs were not increased much with increasing temperature. In contrast, settling velocities of HVFRs increased significantly with increasing

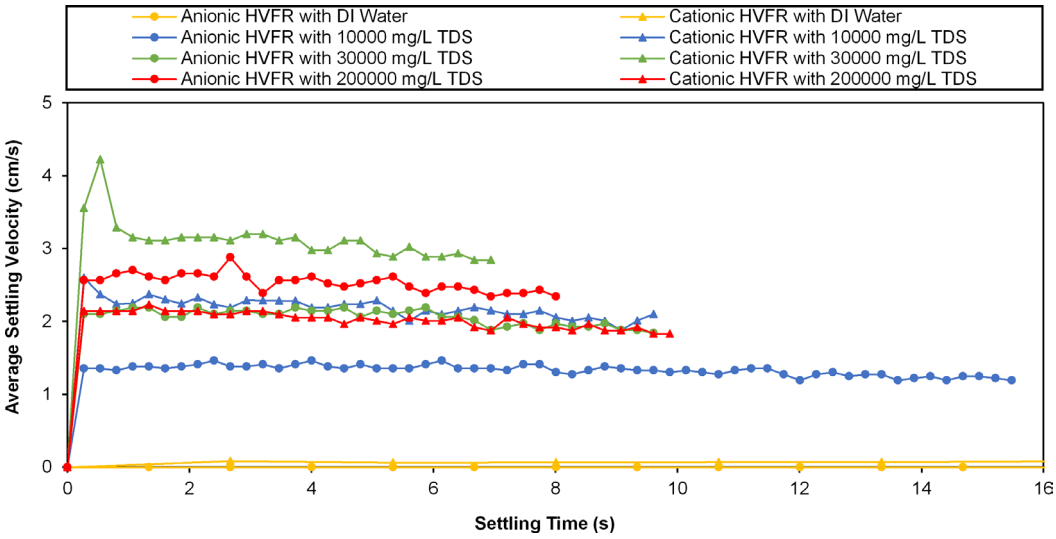

Fig. 8—Unconfined single proppant settling velocity of the 4-GPT anionic and cationic HVFRs in DI and high TDS formation water at 25°C by using Tracker 2.0.

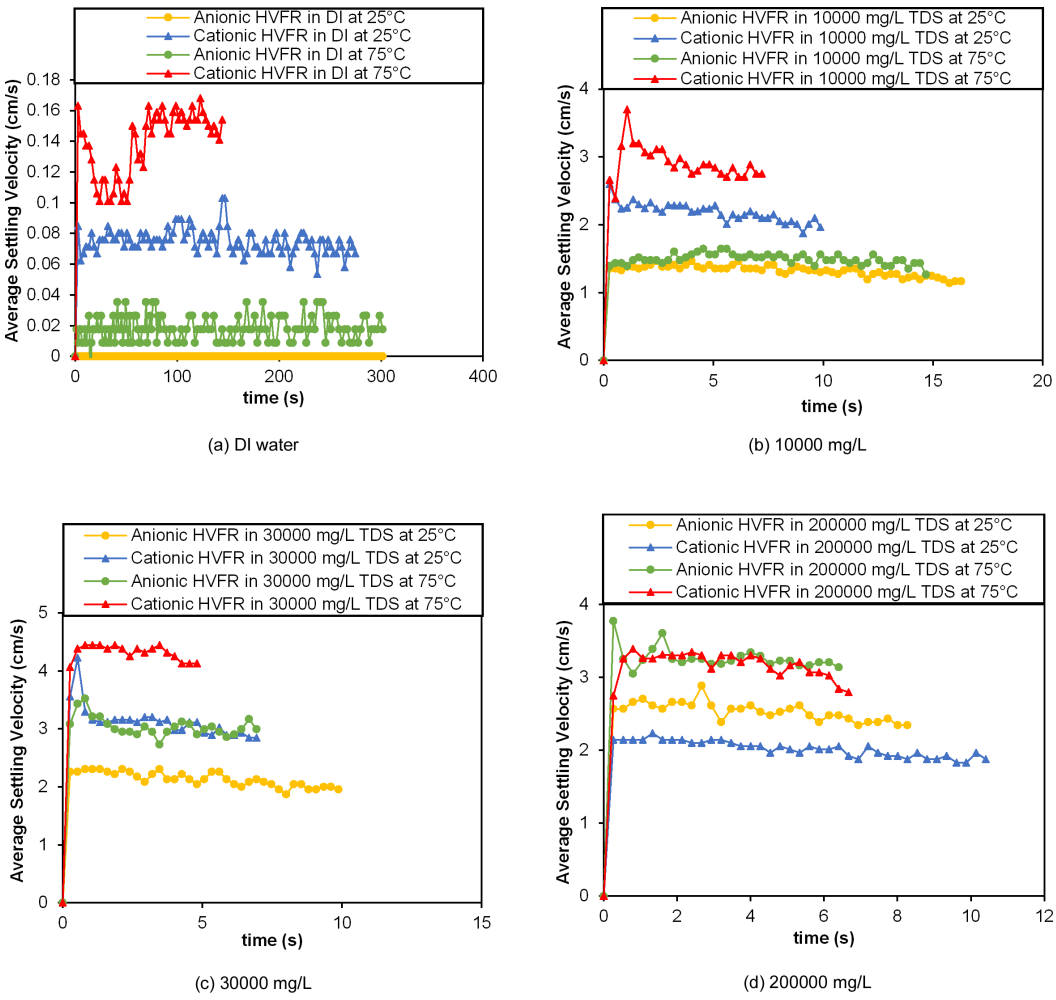

Fig. 9—Unconfined single proppant settling velocity of the 4-GPT anionic and cationic HVFRs in (a) DI water, and (b) 10 000-, (c) 30 000-, and (d) 200 000-mg/L TDS formation water at 25 and 75°C.

Downloaded from http://onepetro.org/SJ/article-pdf/28/02/876/3099587/spe-212298-pa.pdf/1 by Missouri University of Science & Tech user on 09 May 2023

temperature at high TDS condition. High TDS intensified the temperature effect on HVFRs due to the combination of both viscosity and elasticity property changes.

Effect of Wall. **Fig. 10** illustrates the wall-retardation effect on proppant settling velocity in fractures using both anionic and cationic HVFRs with a 3.5-mm fracture width confined model at 25°C. The curves in **Fig. 10a** were also fluctuating due to relatively small settling velocity values. With DI water, settling velocities of the anionic HVFR with and without wall effect were both 0 cm/s. For the cationic HVFR, the settling velocities with and without wall effect were 0.06 and 0.08 cm/s, respectively. In contrast, settling velocities of the anionic HVFR with and without wall effect were 1.2 and 1.9 cm/s at high TDS condition. The settling velocities of the cationic HVFR with and without wall effect were 2.4 and 2.9 cm/s at high TDS condition. The results of the settling velocity into the confined system exhibited the same trend as the velocity in the unconfined model both for the HVFR type and the TDS effects. However, the settling velocity in the confined system was slower than the velocity in the unconfined system. High TDS further intensified the wall effect on proppant settling in HVFRs.

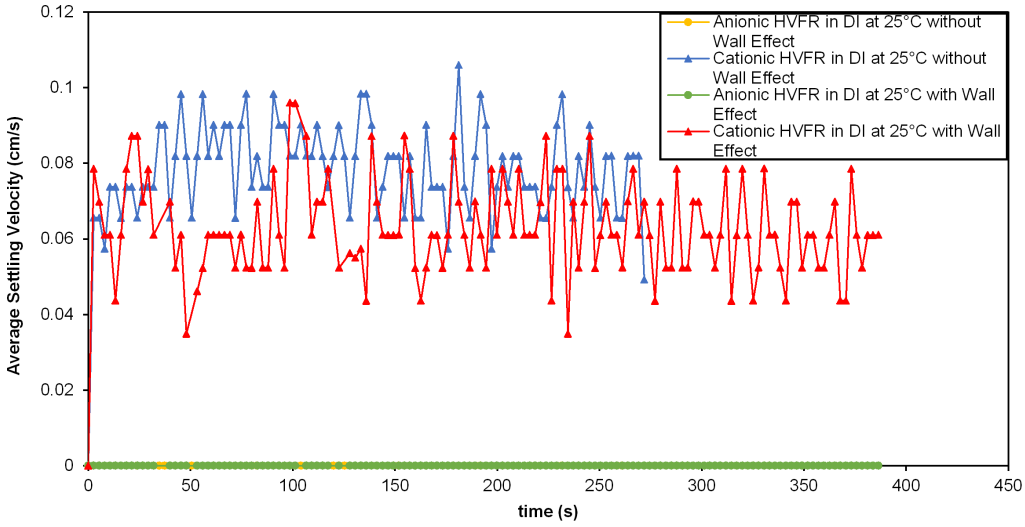

(a) DI water

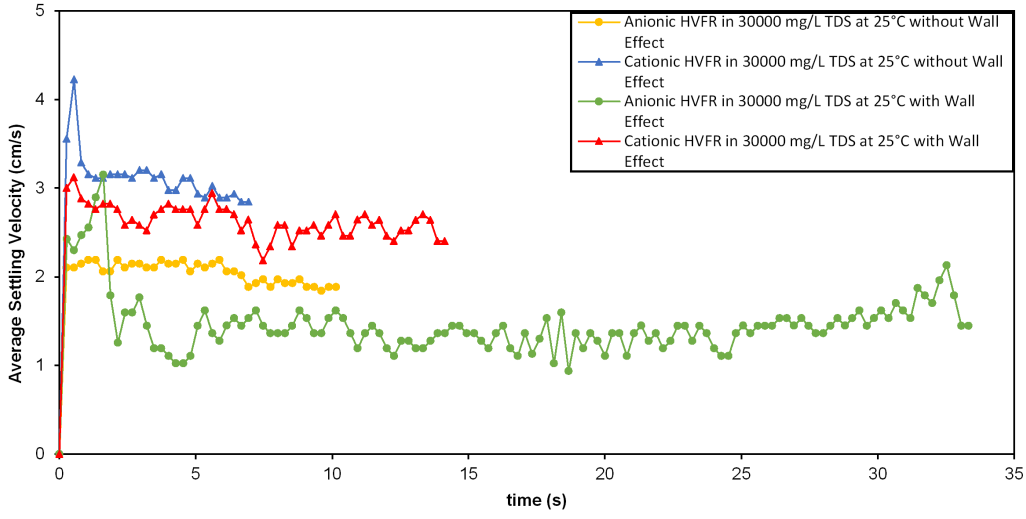

(b) 30000 mg/L TDS

Fig. 10—Unconfined and confined single proppant settling velocities of the 4-GPT anionic and cationic HVFRs in (a) DI water and (b) 30 000-mg/L high TDS formation water at 25°C.

Particle-Hindered Effect. **Fig. 11** qualitatively shows 1 ppg concentration of 30/60 intermediate ceramic proppant settling in both anionic and cationic HVFRs in DI water and 30 000-mg/L high TDS formation water conditions at 25°C. With DI water, the anionic HVFR had much longer settling time than the cationic HVFR. With high TDS formation water, the settling time of both HVFRs decreased significantly and the anionic HVFR had close settling performances with the cationic HVFR, even though the settling time was still longer. All these results matched up with previous single particle settling experiments and the rheology data.

To further investigate the particle-hindered effect, PIV methods were used to describe quantitatively proppant settling as shown in **Fig. 12** and Fig. S-3 in the Supplementary Material. For each figure, part (a) presents the real situation of proppant settlings at certain timings, and part (b) is the settling velocity distribution generated by OpenPIV at corresponding time frames. The *x*-axis represents the width of the cylinder tube, which was 0.03 m. The *y*-axis represents the height of the cylinder tube, which was 0.225 m. However, the investigation area was only from 0 to 0.17 m to avoid proppant sedimentation part at the bottom of the tube. The color bar represents the settling velocity in units of meter per second. The point of *x*, *y* position of 0.015 and 0.15 was selected to further investigate the settling

Downloaded from http://onepetro.org/SJ/article-pdf/28/02/876/3099587/spe-212298-pa.pdf/1 by Missouri University of Science & Tech user on 09 May 2023

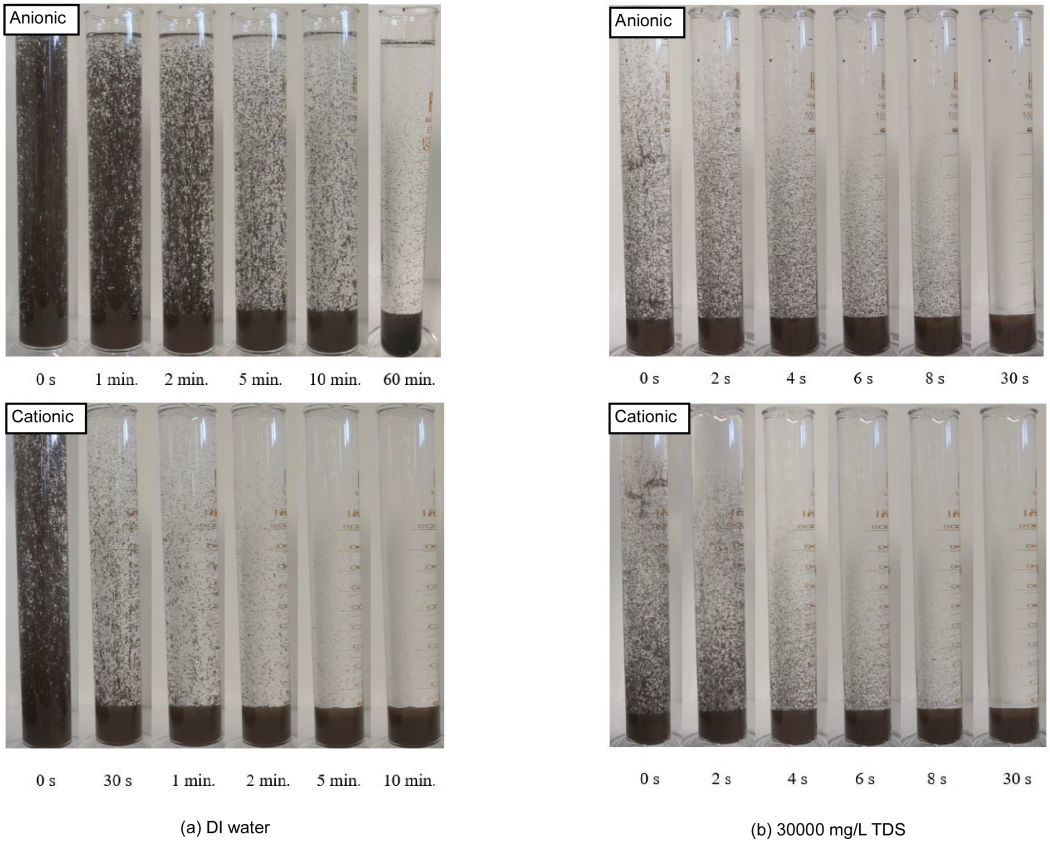

Fig. 11—The schematic of 1 ppg of 30/60 intermediate ceramic proppant settling in the 4-GPT anionic and cationic HVFRs in (a) DI water and (b) 30 000-mg/L TDS formation water at 25°C.

velocities of proppant. As shown in **Fig. 12b**, the settling velocities of the anionic HVFR in 30 000-mg/L high TDS formation water at the selected point for time frames of 1, 3, 5, and 7 seconds were 0.8, 1.44, 1.49, and 1.27 cm/s, which were slightly less than the unconfined single proppant settling velocity of 1.9 cm/s at same TDS condition. Besides, at the time frame of 1 second, the settling velocity distribution had almost zero settling velocity on the right side. This was mainly because some small turbulences were generated by pouring the HVFR fluids with proppant along the left side of the tube, which could bring proppant upward on the right side at the beginning of the experiment. As time went by, the settling velocity on the top of 3-, 5-, and 7-second graphs dropped to zero due to little proppant remaining in these parts.

As shown in Fig. S-3b in the Supplementary Material, the settling velocities of the cationic HVFR in 30 000- mg/L high TDS formation water at the selected point for time frames of 1, 3, 5, and 7 seconds were 2.37, 2.63, 2.1, and 1.7 cm/s, respectively, which were slightly less than the unconfined single proppant settling velocity of 2.9 cm/s at the same TDS condition. On the right side of each graph, there are several blue bar areas which indicate zero settling velocity. This was mainly due to the volume marks on the cylinder tube. Therefore, it was highly suggested that fully transparent fluid containers should be used when doing PIV analysis. To sum up, the accuracy of the PIV method was highly dependent on the quality and arrangement of the equipment. The light profile should be kept the same during recording. Otherwise, noisy points would show up on the results. Also, the PIV method compares the differences between two interrogation regions to determine displacement and velocity; therefore, time frame Δt, the size of interrogation regions, and the overlap would significantly affect the accuracy of results (Scharnowski and Kähler 2020).

In general, sedimentation of proppant was influenced by other particles, and hindered settling was observed. Multiparticles reduced the settling velocity of proppant in both the anionic and cationic HVFRs. Compared with single drop, the differences between anionic and cationic HVFRs were even smaller. Also, the settling velocities of both anionic and cationic HVFRs decreased with increasing time as a result of changing proppant concentrations. Therefore, different proppant concentrations (i.e., 0.5 and 2 ppg) rather than 1 ppg can be chosen to further investigate the proppant concentration effect on the settling velocity in HVFRs.

Dynamic Proppant Settling Measurement. Fig. 13 illustrates the dynamic process of 1 ppg 30/60 intermediate ceramic proppant settling in both anionic and cationic HVFRs in DI water and high TDS formation water conditions with constant injection rate of 2 gal/min and temperature of 75°C.

Two main parameters, peak proppant bank height (H_p) and the distance to injection point (D), were measured and analyzed. The summary of results is plotted in **Fig. 14.** At DI water condition and high TDS up to 30 000 mg/L, the anionic HVFR overall had less peak proppant bank height and longer distance to the injection point than the cationic HVFR, which indicated better proppant transport capability. Furthermore, the presence of high TDS increased the peak proppant bank height and shortened the distance to the injection point for both anionic and cationic HVFRs. Once the TDS level reached 200 000 mg/L, the peak proppant bank of the anionic HVFR only increased slightly and the distance to the injection point stayed constant. In contrast, the peak proppant bank of the cationic HVFR decreased and was lower than the anionic one; the distance to the injection point increased and was higher than the anionic HVFR. All these results generally matched up with previous static particle settling experiments and the rheology data. The anionic HVFR had better proppant transport performance than the cationic one in DI water and high TDS levels below the critical salinity point conditions at 75°C

Downloaded from http://onepetro.org/SJ/article-pdf/28/02/876/3099587/spe-212298-pa.pdf/1 by Missouri University of Science & Tech user on 09 May 2023

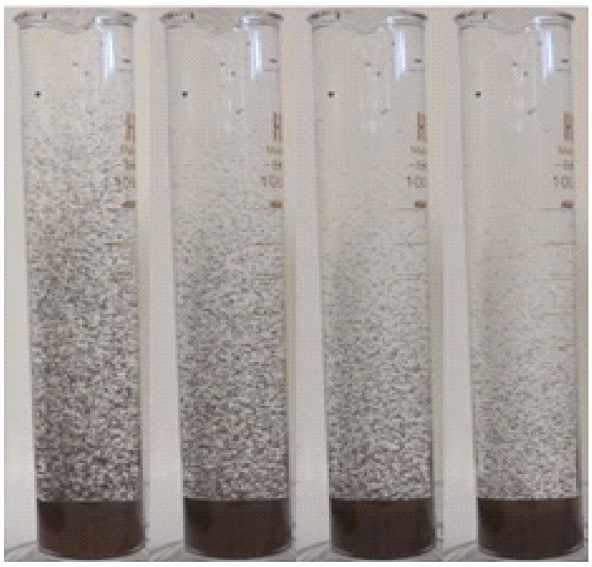

(a) Proppant settling

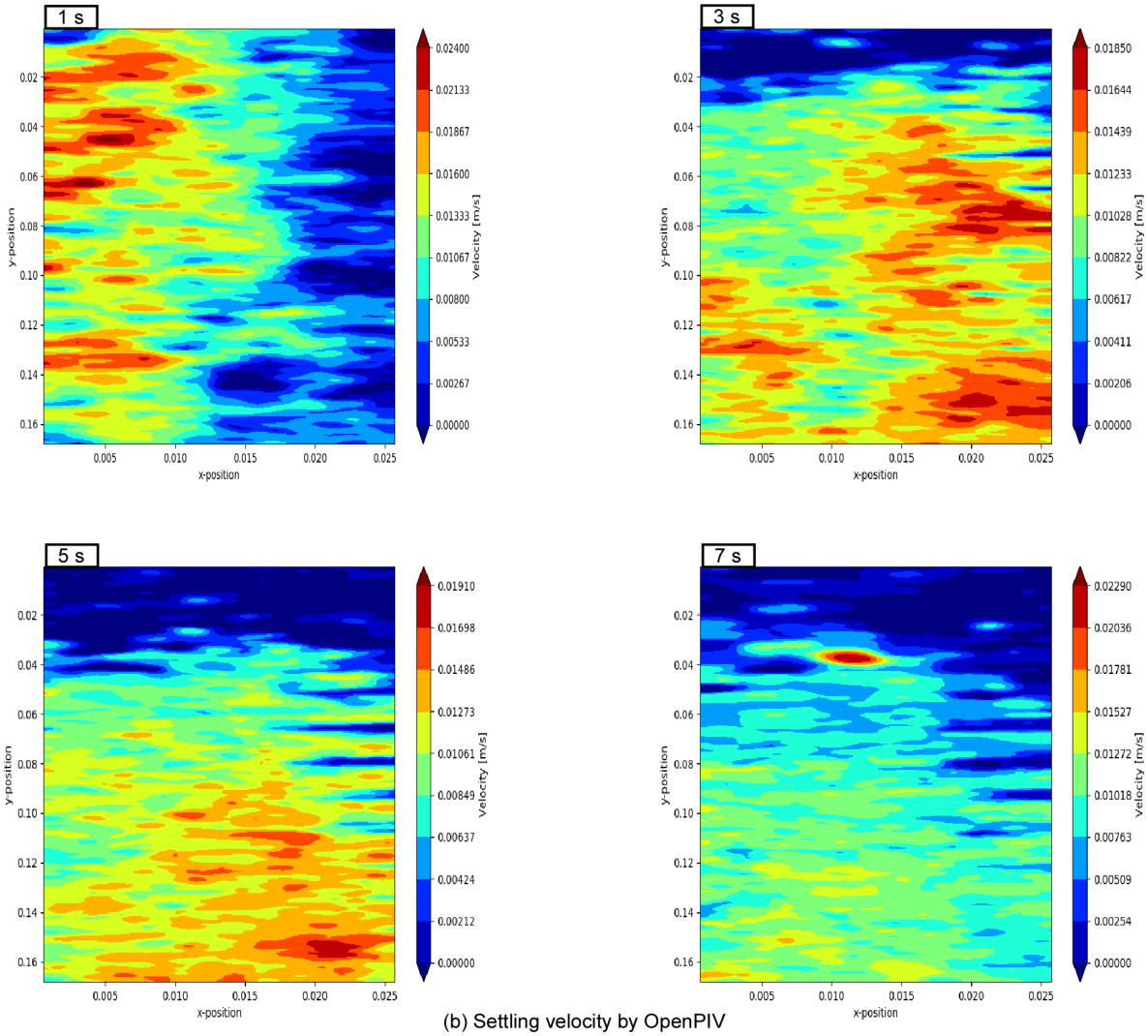

(b) Settling velocity by OpenPIV

Fig. 12—(a) The schematic of 1 ppg of 30/60 intermediate ceramic proppant settling and (b) settling velocity by OpenPIV in the 4-GPT anionic HVFR with 30 000-mg/L high TDS formation water at 25°C. (Note: The 1-second time frame shows the effect of pouring the slurry along the left side of the tube, pushing the proppant up on the right side, and causing nearly zero or negative settling velocity on the right side.)

Downloaded from http://onepetro.org/SJ/article-pdf/28/02/876/3099587/spe-212298-pa.pdf/1 by Missouri University of Science & Tech user on 09 May 2023

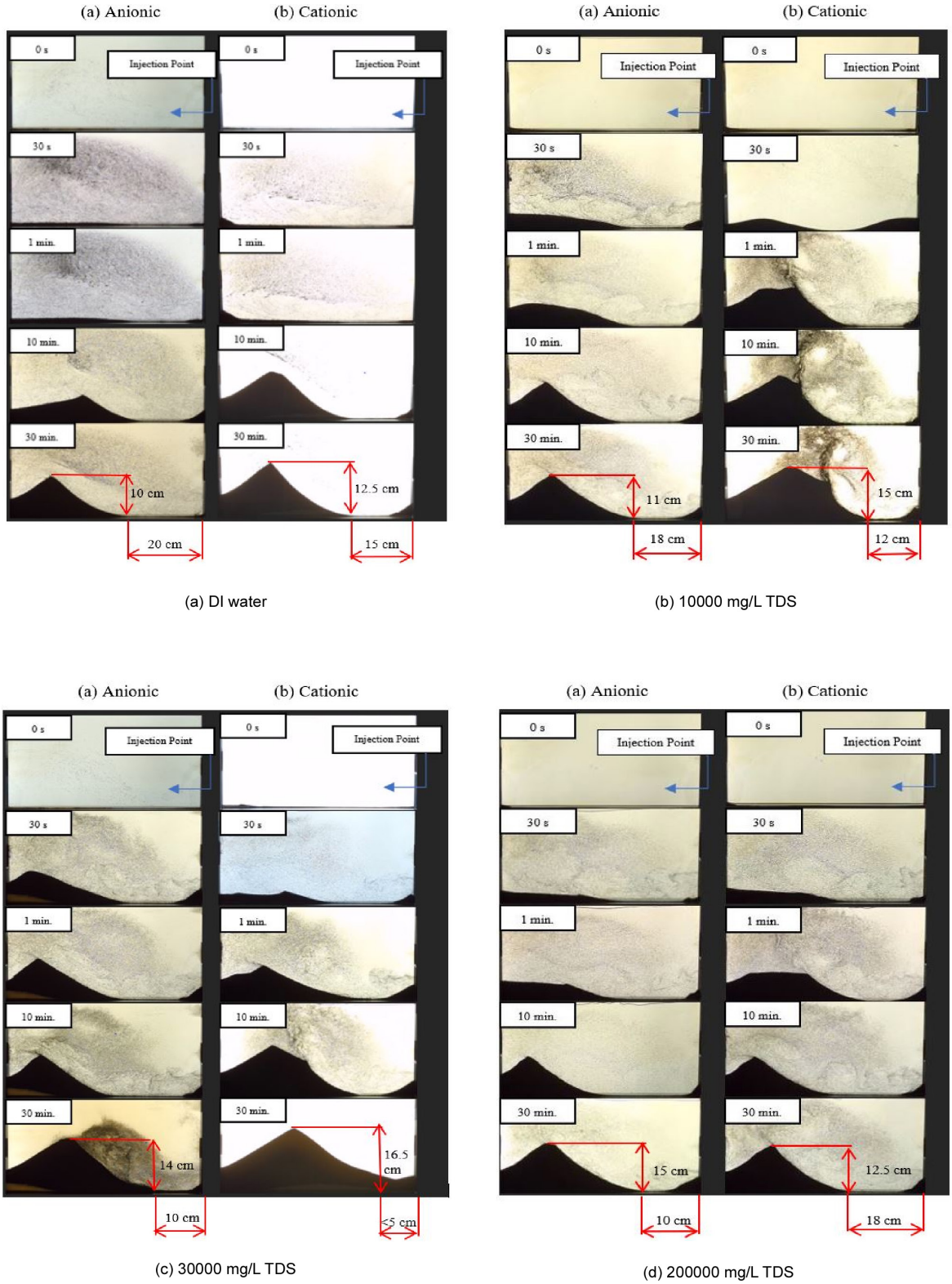

Fig. 13—The schematic of 1 ppg of 30/60 intermediate ceramic proppant dynamic settling in the 4-GPT anionic and cationic HVFRs with (a) DI water and (b) 10 000-, (c) 30 000-, and (d) 200 000-mg/L TDS formation water at 75°C with injection rate of 2 gal/min.

reservoir temperature. Once the TDS level increased above the critical salinity point, the cationic HVFR had better proppant transport performance instead.

However, dynamic proppant transport results may not fully explain the proppant transport capability of HVFRs due to rheology differences. Unlike rheology tests or static settling experiments, experimental variables of dynamic proppant transport were hard to control. The first main uncontrolled factor was mechanical degradation of HVFR polymers during pumping. Long polymer chains were broken by high shear stress, which resulted in rheology property changes. Moreover, the shape of proppant bank (i.e., the peak height of proppant bank, the distance to the injection point, etc.) was determined by a lot of other factors including proppant properties, size of fracture model, and

Downloaded from http://onepetro.org/SJ/article-pdf/28/02/876/3099587/spe-212298-pa.pdf/1 by Missouri University of Science & Tech user on 09 May 2023

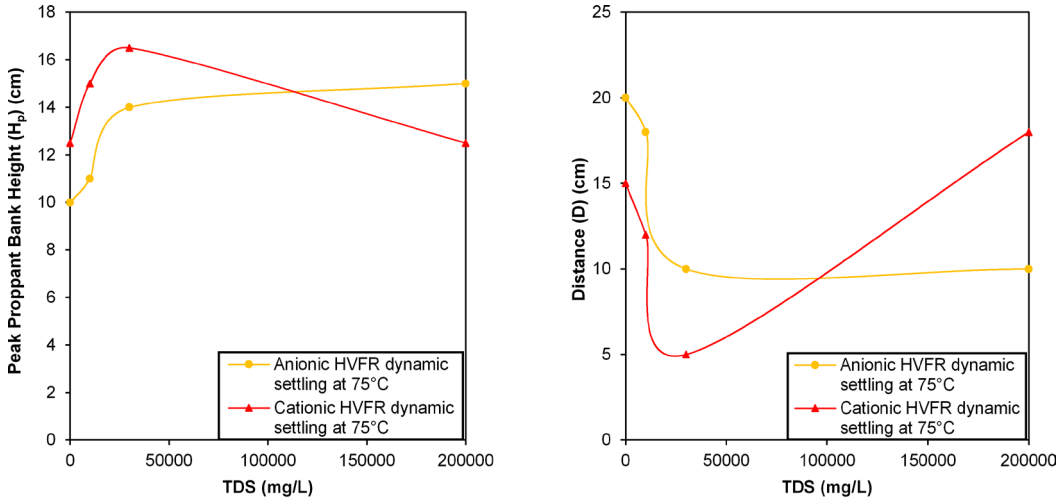

(a) Peak proppant bank height

(b) Distance to injection point

Fig. 14—(a) Peak proppant bank height and (b) distance to injection point of 1 ppg of 30/60 intermediate ceramic proppant dynamic settling in the 4-GPT anionic and cationic HVFRs with DI water and high TDS formation water at 75°C with injection rate of 2 gal/min.

pumping rate. Proppant particles were transported along the surface of proppant bank by rolling, saltation, and suspension, which is known as the bed load transport mechanism. It has been observed as a dominant process in laboratory studies of dynamic proppant transport through a fracture slot according to McClure (2018). Based on McClure's model, the fracture slot was divided into three different regions, which included a near-inlet region, a viscous drag region, and a bed load transport region. The proppant transport mechanism behind each region and how the equilibrium bed height (or the peak bed height) was reached were specifically discussed (McClure 2018).

In terms of our research study, the schematic of general dynamic proppant transport process is shown in **Fig. 15,** where H_b is the height of the bed load transport region. HVFRs with proppant were injected at the bottom of the slot with flowing rate Q_{in}, which was equal to 2 gal/min, from right to left. At the far right, the proppant was lifted and transported by the turbulence flow near the inlet. This region had negligible proppant bed, and the length of this area was marked as D. Moving forward, there was a viscous drag region. However, the range of this region was hard to determine. Especially for the HVFRs in high TDS formation water, viscous drag was less effective as a proppant transport mechanism due to low viscosity. Moreover, because of the fracture model size limitation, the boundary between proppant bed transport dominant region and viscous drag dominant region was also hard to specify. It was highly suggested to have sufficient length of fracture slot for dynamic proppant transport experiments in the future. Based on the computational fluid dynamics simulation results by Liu et al. (2021), the peak height of proppant bed (H_p) is the function of fracture model height (H), fracture model width (W), injection rate (Q_{in}), proppant properties (P, including size, density, friction coefficient, etc.), fluid density (ρ_f), and fluid viscosity (μ_f). Therefore, analysis of H_p and D for dynamic proppant transport was not able to fully explain that the performance differences of both anionic and cationic HVFRs in DI water and high TDS formation water were due to rheology differences. Instead, the time (t) to reach equilibrium bed height was useful to describe proppant transport capability of HVFRs. Comparing **Fig. 13a** with **Figs. 13b through 13d**, HVFRs in DI water had much higher t than the HVFRs in high TDS formation water because there were less depositions due to relatively high viscosity and elasticity. HVFRs in high TDS formation water reached peak proppant bed in about 10 minutes, but almost 30 minutes was required for HVFRs in DI water. Also, previous studies demonstrated that bed load transport was the dominant mechanism in laboratory conditions, but viscous drag was the

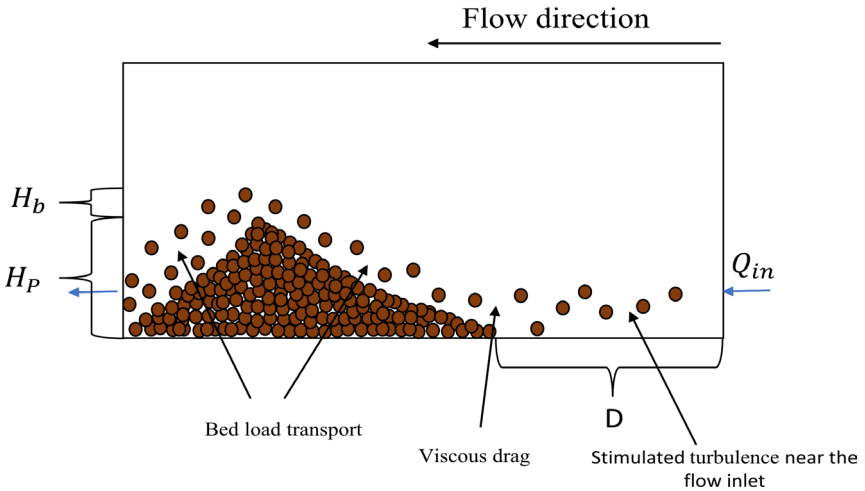

Fig. 15—Schematic of dynamic proppant transport during this research study.

Downloaded from http://onepetro.org/SJ/article-pdf/28/02/876/3099587/spe-212298-pa.pdf/1 by Missouri University of Science & Tech user on 09 May 2023

dominant process at the field scale (McClure 2018). Thus, HVFR studies at relevant field-scale conditions are crucial for successful proppant transport operations. If fracturing results show consistency with the rheology data of HVFRs, then the general decision-making process of selecting HVFRs under high TDS formation water conditions can be simplified to two main steps. In the first step, the rheology properties of HVFRs including viscosity, elasticity, and critical salinity should be determined. In the second step, field tests can be conducted if HVFRs show good rheology properties with high TDS formation water.

During both static and dynamic proppant settling experiments, proppant agglomeration was observed for both anionic and cationic HVFRs in DI water condition as shown in **Fig. 16**. In contrast, it was rare to see in the high TDS condition due to relatively low viscosity. Compared with individual proppant, agglomerated proppant had larger settling velocity (Luo and Tomac 2016). However, HVFRs in DI water still had better overall proppant transport performance than HVFRs in high TDS formation water.

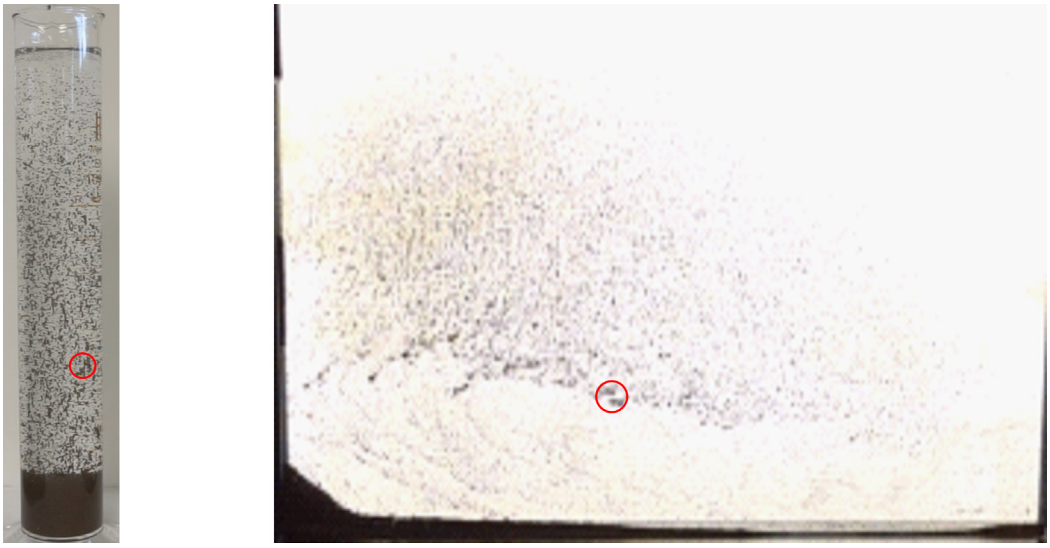

Fig. 16—Proppant agglomeration during static (left) and dynamic (right) proppant settling experiments in the 4-GPT anionic HVFR with DI water.

Conclusions

An anionic HVFR and a cationic HVFR were tested under different TDS and temperature conditions. Based on the results, the following conclusions can be drawn:

- Under DI water condition, the anionic HVFR has higher viscosity than the cationic HVFR due to larger molecular weight and has much higher elasticity. Adding high level of TDS decreases the viscosity and elasticity profiles of both anionic and cationic HVFRs. Especially for the elasticity, it is negligible for both HVFRs even with 10 000-mg/L TDS. However, high TDS has more side effects on viscosity of the anionic HVFR than the cationic HVFR for TDS level below critical salinity, even though the anionic one has higher average values. Once the TDS level is above critical salinity, the viscosity of both HVFRs increases, and the cationic HVFR has higher viscosity than the anionic one due to lower critical salinity" point.
- Temperature also has significant effects on the viscosity of anionic and cationic HVFRs. Increasing temperature decreases the viscosity of HVFRs, and the fluids become even more unstable. High TDS concentration intensifies the temperature effect on the thermal stability of HVFRs, and this effect is more significant for the anionic HVFR.
- Static proppant settling experiments match well with fluid rheology data. Both viscosity and elasticity contribute to the proppant transport capacity of HVFRs. However, at high TDS conditions, the function of elasticity is negligible. The wall effect and the particle-hindered effect are observed for both anionic and cationic HVFRs in DI water and high TDS formation water conditions. Both effects decrease the settling velocity of proppant in HVFRs.
- Dynamic proppant settling experiment results have positive correlation with fluid rheology data. However, many other factors, including polymer degradation and bed load transport mechanism, also affect performance of proppant transported in the slot. It is highly recommended to have sufficient length of fracture model to execute this kind of experiments and add time scale to better describe the results.
- The general decision-making process of selecting HVFRs under high TDS formation water conditions can be simplified to two main steps. In the first step, the rheology properties of HVFRs, including viscosity, elasticity, and critical salinity, should be determined. In the second step, field tests can be conducted if HVFRs show good rheology properties with high TDS formation water.
- Proppant agglomeration is observed for both anionic and cationic HVFRs in DI water condition but seldom noticeable in the high TDS conditions. Compared with individual proppant, agglomerated proppant has larger settling velocity. However, HVFRs in DI water still have better overall proppant transport performance than HVFRs in high TDS formation water.
- The PIV method can be used to quantitatively analyze static settling of multiparticles and precisely determine their settling velocities, even for particles as small as proppant. However, the accuracy of the PIV method is highly dependent on the quality and arrangement of the equipment. Future study can be focused on quantitatively analyzing dynamic proppant transport by using PIV method to provide more test data for simulation work.
- Viscosity and elasticity have no correlation with HVFR types (anionic or cationic). They are more related to the polymer's own properties such as molecular weight and molecular structures of the polymer network. In other words, cationic HVFRs do not always have better proppant transport performance than anionic HVFRs under high TDS conditions. However, more anionic and cationic HVFRs in the industrial market remain to be tested under a wide range of TDS levels to fully understand the performance differences between anionic and cationic HVFRs with high TDS formation water and to draw more general conclusions. Questions, such as the

Downloaded from http://onepetro.org/SJ/article-pdf/28/02/876/3099587/spe-212298-pa.pdf/1 by Missouri University of Science & Tech user on 09 May 2023

mechanism behind the TDS effects on the elasticity of HVFRs, whether cations have more effects on anionic HVFRs or anions have more effects on cationic HVFRs, and proppant concentration effects on the settling velocity in HVFRs, can also be studied in future research.

Acknowledgment

The authors wish to thank SNF Holding Company for providing both anionic and cationic HVFR samples. The authors also thank CARBO Company for providing ceramic proppant.

References

Abdullah, M. Z., Odjoji, E., and Angeli, P. 2008. The Effect of Polymer Concentration and Hydration Period on Horizontal Oil-Water Flows. Paper presented at the 11th International Conference on Multiphase Flow in Industrial Plant (MFIP 2008), Palermo, Italy.

Applebey, M. P. 1910. CCXI.—The Viscosity of Salt Solutions. *J Chem Soc Trans* **97**: 2000–2025. https://doi.org/10.1039/CT9109702000.

Arnipally, S. K. and Kuru, E. 2018. Settling Velocity of Particles in Viscoelastic Fluids: A Comparison of the Shear-Viscosity and Elasticity Effects. *SPE J.* **23** (5): 1689–1705. SPE-187255-PA. https://doi.org/10.2118/187255-PA.

Ba Geri, M., Imqam, A., and Flori, R. 2019. A Critical Review of Using High Viscosity Friction Reducers as Fracturing Fluids for Hydraulic Fracturing Applications. Paper presented at the SPE Oklahoma City Oil and Gas Symposium, Oklahoma City, Oklahoma, USA, 9–10 April. SPE-195191-MS. https://doi.org/10.2118/195191-MS.

Biheri, G. and Imqam, A. 2022. Proppant Transport Using High-Viscosity Friction Reducer Fracture Fluids at High-Temperature Environment. *SPE J.* **27** (1): 60–76. SPE-206750-PA. https://doi.org/10.2118/206750-PA.

Das, P. and Rahim, Z. 2014. Evaluate Fracturing Fluid Performance for Hydraulic Stimulation in Pre-Khuff Sandstone Reservoirs of Ghawar Gas Field. Paper presented at the SPE Saudi Arabia Section Technical Symposium and Exhibition, Al-Khobar, Saudi Arabia, 21–24 April. SPE-172217-MS. https://doi.org/10.2118/172217-MS.

Deville, J. P., Fritz, B., and Jarrett, M. 2011. Development of Water-Based Drilling Fluids Customized for Shale Reservoirs. *SPE Drill & Compl* **26** (4): 484–491. SPE-140868-PA. https://doi.org/10.2118/140868-PA.

Downey, J. S. and Armstrong, C. A. 1977. *Ground-Water Resources of Griggs and Steele Counties, North Dakota: North Dakota State Water Commission County Groundwater, Studies 21, Pt III, and North Dakota Geological Survey Bulletin 64, Part III*, 33. Reston, Virginia, USA: United States Geological Survey and North Dakota Geological Survey.

Franck, A. 2003. Measuring Structure of Low Viscosity Fluids in Oscillation Using a Rheometer with and without Separate Torque Transducer. *Annu Trans Nord Rheol Soc* **11**: 95–100.

Galindo, T. 2019. Does Higher Viscosity Improve Proppant Transport? Paper presented at the SPE Oklahoma City Oil and Gas Symposium, Oklahoma City, Oklahoma, USA, 9–10 April. SPE-195192-MS. https://doi.org/10.2118/195192-MS.

Giraldo, J. B., Vermuë, M. H., Olivieri, G. et al. 2016. Understanding the Salinity Effect on Cationic Polymers in Inducing Flocculation of the Microalga Neochloris Oleoabundans. *J Biotechnol* **225**: 10–17. https://doi.org/10.1016/j.jbiotec.2016.03.009.

Haghshenas, A. and Nasr-El-Din, H. A. 2014. Effect of Dissolved Solids on Reuse of Produced Water at High Temperature in Hydraulic Fracturing Jobs. *J Nat Gas Sci Eng* **21**: 316–325. https://doi.org/10.1016/j.jngse.2014.08.013.

Harris, P. C., Morgan, R. G., and Heath, S. J. 2005. Measurement of Proppant Transport of Frac Fluids. Paper presented at the SPE Annual Technical Conference and Exhibition, Dallas, Texas, USA, 9–12 October. SPE-95287-MS. https://doi.org/10.2118/95287-MS.

Hu, Y. T., Fisher, D., Kurian, P. et al. 2018. Proppant Transport by a High Viscosity Friction Reducer. Paper presented at the SPE Hydraulic Fracturing Technology Conference and Exhibition, The Woodlands, Texas, USA, 23–25 January. SPE-189841-MS. https://doi.org/10.2118/189841-MS.

Huh, C., Bryant, S. L., Sharma, M. M. et al. 2009. PH Sensitive Polymers for Novel Conformance Control and Polymerflood Applications. Paper presented at the SPE International Symposium on Oilfield Chemistry, The Woodlands, Texas, USA, 20–22 April. SPE-121686-MS. https://doi.org/10.2118/121686-MS.

Johnson, M., Winkler, A., Aften, C. et al. 2018. Successful Implementation of High Viscosity Friction Reducer in Marcellus Shale Stimulation. Paper presented at the SPE/AAPG Eastern Regional Meeting, Pittsburgh, Pennsylvania, USA, 7–11 October. SPE-191774-18ERM-MS. https://doi.org/10.2118/191774-18ERM-MS.

Kakadjian, S., Thompson, J., and Torres, R. 2015. Fracturing Fluids from Produced Water. Paper presented at the SPE Production and Operations Symposium, Oklahoma City, Oklahoma, USA, 1–5 March. SPE-173602-MS. https://doi.org/10.2118/173602-MS.

Kresse, T. M., Warner, N. R., Hays, P. D. et al. 2012. *Shallow Groundwater Quality and Geochemistry in the Fayetteville Shale Gas-Production Area, North-Central Arkansas, 2011*, 2012–5273. Reston, Virginia, USA: US Department of the Interior, US Geological Survey. https://doi.org/10.3133/sir20125273.

Kurtoglu, B., Kazemi, H., Rosen, R. et al. 2014. A Rock and Fluid Study of Middle Bakken Formation: Key to Enhanced Oil Recovery. Paper presented at the SPE/CSUR Unconventional Resources Conference – Canada, Calgary, Alberta, Canada, 30 September–2 October. SPE-171668-MS. https://doi.org/10.2118/171668-MS.

Liang, F., Sayed, M., Al-Muntasheri, G. A. et al. 2016. A Comprehensive Review on Proppant Technologies. *Petroleum* **2** (1): 26–39. https://doi.org/10.1016/j.petlm.2015.11.001.

Liu, Y. and Sharma, M. M. 2005. Effect of Fracture Width and Fluid Rheology on Proppant Settling and Retardation: An Experimental Study. Paper presented at the SPE Annual Technical Conference and Exhibition, Dallas, Texas, USA, 9–12 October. SPE-96208-MS. https://doi.org/10.2118/96208-MS.

Liu, C., Li, M., Zhang, G. et al. 2021. Quantitative Study on Bed Load Proppant Transport during Slickwater Hydraulic Fracturing. *Lithosphere* **2021** (Special 1): 9207672. https://doi.org/10.2113/2021/9207672.

Løbø Viken, A., Skauge, T., and Spildo, K. 2016. Rheological Properties of a Hydrophobically Modified Anionic Polymer: Effect of Varying Salinity and Amount of Hydrophobic Moieties. *J Appl Polym Sci* **133** (23). https://doi.org/10.1002/app.43520.

Loveless, D., Holtsclaw, J., Saini, R. et al. 2011. Fracturing Fluid Comprised of Components Sourced Solely from the Food Industry Provides Superior Proppant Transport. Paper presented at the SPE Annual Technical Conference and Exhibition, Denver, Colorado, USA, 30 October–2 November. SPE-147206-MS. https://doi.org/10.2118/147206-MS.

Luo, L. and Tomac, I. 2016. Particle Image Velocimetry Analysis of Proppant Settling in a Narrow Slot. Paper presented at the 50th U.S. Rock Mechanics/Geomechanics Symposium, Houston, Texas, USA, 26–29 June. ARMA-2016-652.

McClure, M. 2018. Bed Load Proppant Transport during Slickwater Hydraulic Fracturing: Insights from Comparisons between Published Laboratory Data and Correlations for Sediment and Pipeline Slurry Transport. *J Pet Sci Eng* **161**: 599–610. https://doi.org/10.1016/j.petrol.2017.11.043.

Downloaded from http://onepetro.org/SJ/article-pdf/28/02/876/3099587/spe-212298-pa.pdf/1 by Missouri University of Science & Tech user on 09 May 2023

McDonald, B. and Wright, T. H. 2016. Completion Optimization in the Fayetteville Shale Utilizing Rate Transient Analysis for Candidate Selection. Paper presented at the SPE Hydraulic Fracturing Technology Conference, The Woodlands, Texas, USA, 9–11 February. SPE-179160-MS. https://doi.org/10.2118/179160-MS.

Nasr-El-Din, H. A. and Taylor, K. C. 1996. Rheology of Water-Soluble Polymers Used for Improved Oil Recovery. In *Advances in Engineering Fluid Mechanics: Multiphase Reactor and Polymerization System Hydrodynamics*, 615–668. Amsterdam, The Netherlands: Elsevier. https://doi.org/10.1016/B978-088415497-6/50026-7.

Padhy, S., Shaqfeh, E. S. G., Iaccarino, G. et al. 2013. Simulations of a Sphere Sedimenting in a Viscoelastic Fluid with Cross Shear Flow. *J Non-Newton Fluid Mech* **197**: 48–60. https://doi.org/10.1016/j.jnnfm.2013.02.003.

Palisch, T. T., Vincent, M. C., and Handren, P. J. 2010. Slickwater Fracturing: Food for Thought. *SPE Prod & Oper* **25** (3): 327–344. SPE-115766-PA. https://doi.org/10.2118/115766-PA.

Panyukov, S. 2020. Theory of Flexible Polymer Networks: Elasticity and Heterogeneities. *Polymers (Basel)* **12** (4). https://doi.org/10.3390/polym12040767.

Sahai, R. and Moghanloo, R. G. 2019. Proppant Transport in Complex Fracture Networks – A Review. *J Pet Sci Eng* **182**: 106199. https://doi.org/10.1016/j.petrol.2019.106199.

Scharnowski, S. and Kähler, C. J. 2020. Particle Image Velocimetry - Classical Operating Rules from Today's Perspective. *Opt Lasers Eng* **135**: 106185. https://doi.org/10.1016/j.optlaseng.2020.106185.

Seright, R. S., Campbell, A. R., Mozley, P. S. et al. 2010. Stability of Partially Hydrolyzed Polyacrylamides at Elevated Temperatures in the Absence of Divalent Cations. *SPE J.* **15** (2): 341–348. SPE-121460-PA. https://doi.org/10.2118/121460-PA.

Shah, S. N. 1993. Rheological Characterization of Hydraulic Fracturing Slurries. *SPE Prod & Fac* **8** (2): 123–130. SPE-22839-PA. https://doi.org/10.2118/22839-PA.

Shen, L., Khan, S., Heller, D. et al. 2019. A Cationic Friction Reducer Fully Compatible with Produced Water. Paper presented at the SPE/AAPG/SEG Unconventional Resources Technology Conference, Denver, Colorado, USA, 22–24 July. URTEC-2019-129-MS. https://doi.org/10.15530/urtec-2019-129.

Thyne, G. and Brady, P. 2016. Evaluation of Formation Water Chemistry and Scale Prediction: Bakken Shale. *Appl Geochem* **75**: 107–113. https://doi.org/10.1016/j.apgeochem.2016.10.015.

Walters, H. G., Stegent, N. A., and Harris, P. C. 2009. New Frac Fluid Provides Excellent Proppant Transport and High Conductivity. Paper presented at the SPE Hydraulic Fracturing Technology Conference, The Woodlands, Texas, USA, 19–21 January. SPE-119380-MS. https://doi.org/10.2118/119380-MS.

Ward, J. S. and Martin, F. D. 1981. Prediction of Viscosity for Partially Hydrolyzed Polyacrylamide Solutions in the Presence of Calcium and Magnesium Ions. *SPE J.* **21** (5): 623–631. SPE-8978-PA. https://doi.org/10.2118/8978-PA.

Williams, H., Khatri, D., Keese, R. et al. 2011. Flexible, Expanding Cement System (FECS) Successfully Provides Zonal Isolation Across Marcellus Shale Gas Trends. Paper presented at the Canadian Unconventional Resources Conference, Calgary, Alberta, Canada, 15–17 November. SPE-149440-MS. https://doi.org/10.2118/149440-MS.

Yamashiro, B. D. and Tomac, I. 2020. Proppant Slurry Flow and Transport within Fractures with Rough Surfaces. Paper presented at the 54th U.S. Rock Mechanics/Geomechanics Symposium, Virtual, 28 June–1 July. ARMA-2020-1291.

Zhu, Z., Song, X., Yao, X. et al. 2021. Intelligent Prediction of Settling Velocity for Arbitrary Shape Particles in Vertical Fractures. Paper presented at the 55th U.S. Rock Mechanics/Geomechanics Symposium, Virtual, 18–25 June. ARMA-2021-1025.

Downloaded from http://onepetro.org/SJ/article-pdf/28/02/876/3099587/spe-212298-pa.pdf/1 by Missouri University of Science & Tech user on 09 May 2023